Univerzita Karlova

Přírodovědecká fakulta

Studijní program: Medicinální chemie

Bc. Jáchym Hrušák

Syntéza fluorogenních tetrazinů s červeným posunem pro aplikace v biologickém zobrazování

Synthesis of red-shifted fluorogenic tetrazines for bioimaging applications

Typ závěrečné práce:

Diplomová práce

Vedoucí práce/Školitel:

Ing. Milan Vrábel, Ph.D

Praha, 2025

Prohlášení:

Prohlašuji, že jsem závěrečnou práci zpracoval samostatně a že jsem uvedl všechny použité informační zdroje a literaturu. Tato práce ani její podstatná část nebyla předložena k získání jiného nebo stejného akademického titulu.

V Praze, 13.5.2025

Podpis

Abstrakt

Použití fluorogenních sond pro fluorescenční zobrazování v biologii přitahuje pozornost vědecké komunity již několik desetiletí.[1] Představení konceptu bioortogonální chemie skupinou Carolyn Bertozzi[2] v roce 2003 poskytlo nový vhled do světa fluorogenních sond a podnítilo rozvoj různých oblastí chemie a chemické biologie. Fluorogenní sondy nevykazují fluorescenci, dokud nedojde k jejich specifické aktivaci, což umožňuje zobrazování bez potřeby oplachování s vynikajícím poměrem signálu k šumu.[3] V této práci jsem se zaměřil na návrh, syntézu a aplikaci nových fluorogenních sond s červeným posunem založených na **BODIPY-FL**. Fluorogenní vlastnosti těchto sond byly zkoumány pomocí fotofyzikálních experimentů a vybrané sloučeniny byly dále testovány v biologickém zobrazování živých buněk.

Klíčová slova: bioortogonální chemie, BODIPY, červený posun, fluorogenní sondy, tetraziny, triaziniové soli.

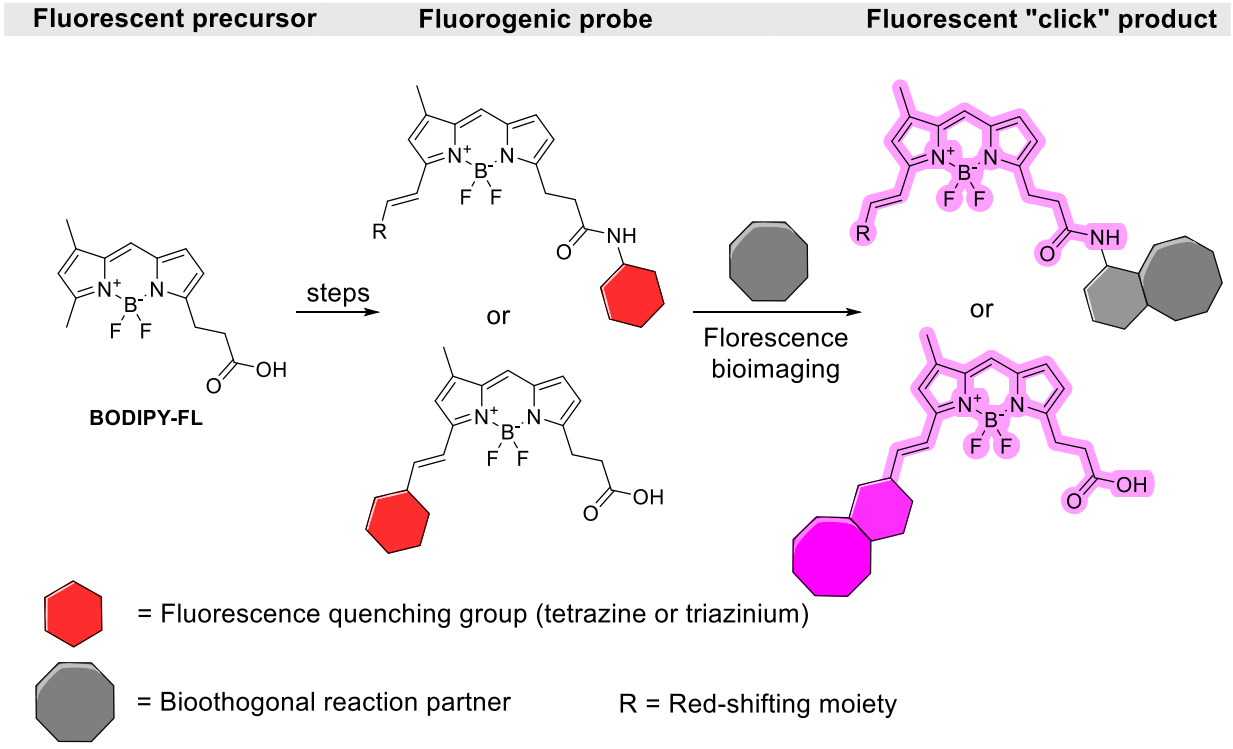

Abstract

The use of fluorogenic probes in fluorescence bioimaging has attracted much attention over the past few decades.[1] The introduction of bioorthogonal chemistry by Bertozzi in 2003[2] provided a new perspective on fluorogenicity and spurred the development of various branches of chemistry and chemical biology. Fluorogenic probes are non-fluorescent until specific activation, enabling no-wash imaging protocols with exceptional signal-to-noise ratios.[3] In this work, I focused on the design, synthesis, and application of novel **BODIPY-FL**-based red-shifted fluorogenic probes. The fluorogenic properties of these probes were evaluated through photophysical studies and selected compounds were further tested in live-cell bioimaging experiments.

Key words: Bioorthogonal chemistry, BODIPY, fluorogenic probes, red-shift, tetrazines, triazinium salts.

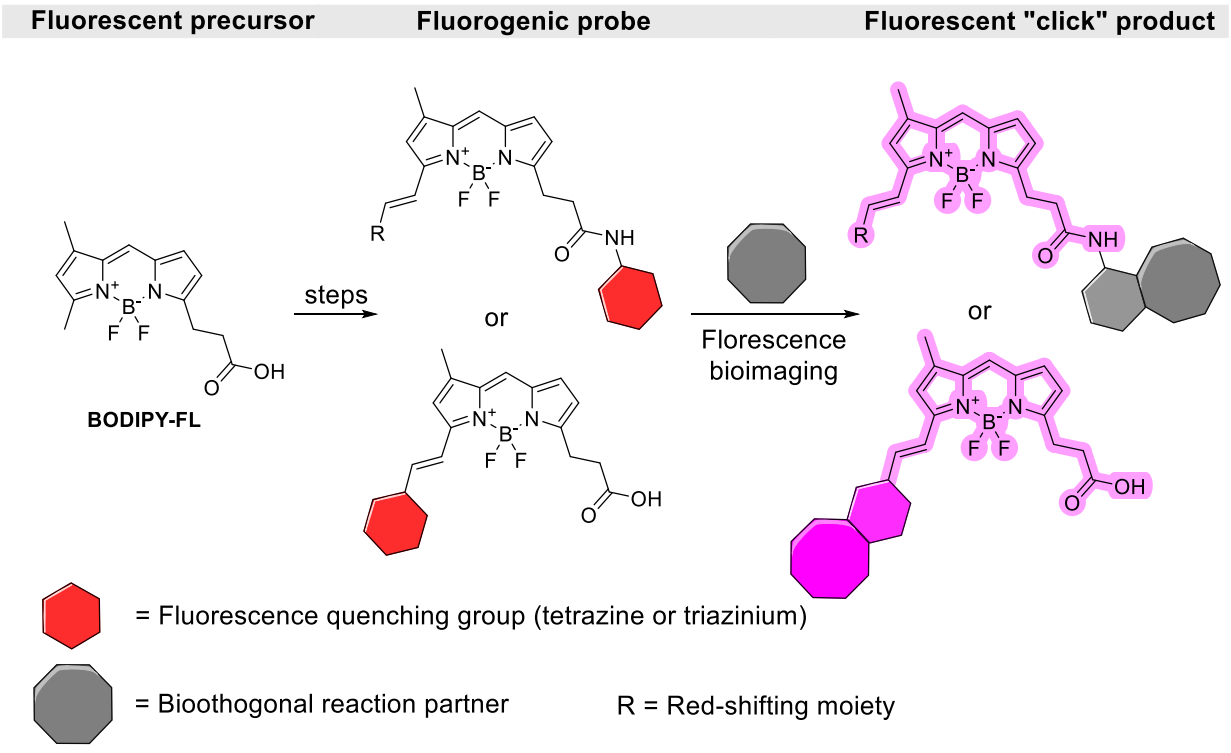

Table of Contents

Abbreviations

Ac	Acetyl
BCN	Bicyclo[6.1.0]non-4-yne
Boc	*tert*-Butyloxycarbonyl
BODIPY	4,4-Difluoro-4-bora-3a,4a-diaza-s-indacene
DA	Diels-Alder reaction
DCM	Dichloromethane
DET	Dexter electron transfer
DFT	Density functional theory
DIPEA	Diisopropylethyl amine
DMEM	Dulbecco's modified Eagle medium
DMF	Dimethylformamide
DMP	Dess-Martin periodinane
DMSO	Dimethylsulfoxide
EnT	Energy transfer
Et	Ethyl
ETDS	Energy transfer to a dark state
FE	Fluorescence enhancement
FP	Fluorescent protein
FRET	Förster resonance energy transfer

GFP	Green fluorescent protein
HATU	Hexafluorophosphate azabenzotriazole tetramethyluronium
HWE	Horner–Wadsworth–Emmons reaction
ICDS	Internal conversion to a dark state
iEDDA	Inverse electron demand Diels–Alder reaction
LCMS	Liquid chromatography–mass spectrometry
Me	Methyl
NIR	Near-infrared
NMR	Nuclear magnetic resonance
PE	Petroleum ether
PEG	Polyethylene glycol
PeT	Photoinduced electron transfer
Ph	Phenyl
RET	Resonance energy transfer
RP	Resversed-phase
SNR	Signal-to-noise ratio
Sph	Spiro[2.3]hex-1-ene
TBET	Through-bond energy transfer
*t*Bu	*tert*-Butyl
TCO	*trans*-Cyclooctene

Tf	Trifluoromethanesulfonyl
TFA	Trifluoroacetic acid
THF	Tetrahydrofuran
TLC	Thin-layer chromatography
TPP	Triphenylphosphonium
Trz^+	Triazinium
Tz	Tetrazine
UV	Ultraviolet

1. Introduction

1.1 Fluorescence bioimaging

Visualization of biomacromolecules *via* fluorescence has been an important tool of biological research over the last few decades. Fluorescence bioimaging enables real-time, non-invasive tracking of cellular processes and molecular interactions with high spatial and temporal resolution.[4] Over the years, many methodologies for fluorescence bioimaging have been developed.

Fluorescent proteins (FPs) are commonly used in molecular biology as fluorescent reporters of gene expression, but genetically modified FPs have also been found to act as biosensors by utilizing the sensitivity of FPs to, for example, pH. In 2008, O. Shimomura, R. Y. Tsien, and M. Chalfie were awarded with the Nobel Prize in chemistry for their discovery and development of the widely used green fluorescent protein – GFP (Figure 1). Fluorescent proteins remain in use particularly due to the fact that the fluorescence is genetically encoded, which means they can be expressed in living cells or organisms. Another type of fluorescent molecules used in fluorescence bioimaging are small molecule dyes. In comparison to organic small molecule dyes, FPs show much lower quantum yields, brightness and photostability.[5]

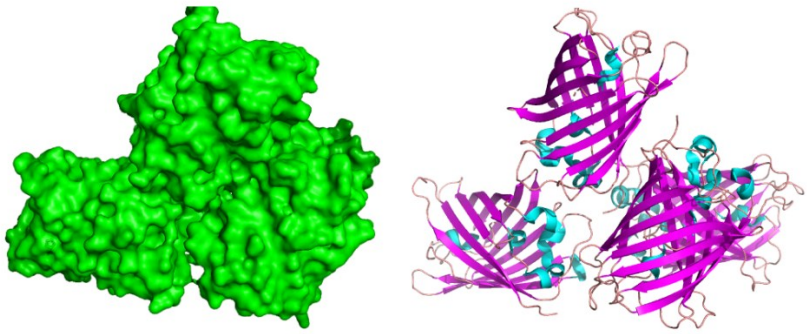

Figure 1: Green fluorescent protein (GFP) in surface (left) and ribbon (right) representation (PDB ID: 2QLE).

In fluorescence microscopy, which enables the study of biological processes *via* fluorescence, signal-to-noise ratio (SNR) is the key aspect of a successful experiment. Among other obstacles, a researcher must deal with with autofluorescence (the intrinsic fluorescence of the studied system), which can produce background noise that compromises the experiment.[1]

1.2 Bioorthogonal chemistry in fluorescence bioimaging

A very attractive way to increase signal-to-noise ratio is the use of fluorogenic probes. Such probes exhibit little to no fluorescence in their initial state, but it is increased significantly after a chemical reaction – a unique property of a chemical compound called fluorogenicity.[1] The need for fluorogenic probes appears mostly in cases when the experiment setup does not allow for washing steps, for example during *in vivo* experiments or live-cell imaging. In such cases, fluorogenic probe allows for specific visualization of the target, while the background fluorescence of the non-activated probe remains low.[3] One of the early example of a fluorogenic compound is Fluo-3 (Figure 2), a dye that, after its activation by intracellular esterases, increases its fluorescence up to 40-fold upon binding Ca^{2+}.[6]

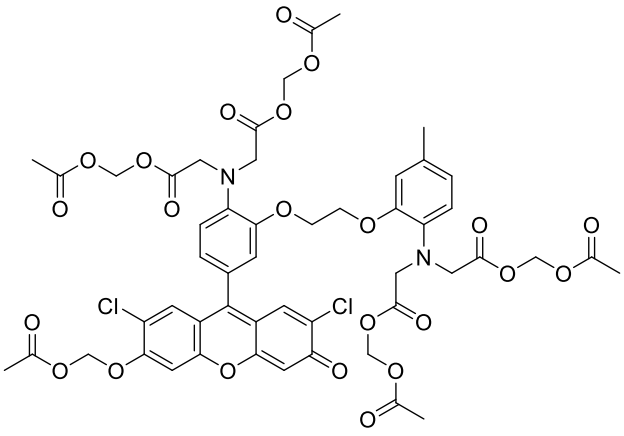

Figure 2: Molecular structure of Fluo-3.

With the introduction of bioorthogonal chemistry, the research of fluorogenic probes skyrocketed. Introduced by the group of Bertozzi in 2003[7], bioorthogonal reactions have revolutionized bioconjugation chemistry, fluorescent labelling as well as many other fields of chemistry and chemical biology.[8–10] These reactions must obey certain rules to be

considered bioorthogonal: fast kinetics, tolerance to aqueous environment, high selectivity and compatibility with naturally occurring functional groups – they are *orthogonal* to biological systems (Figure 3).[8]

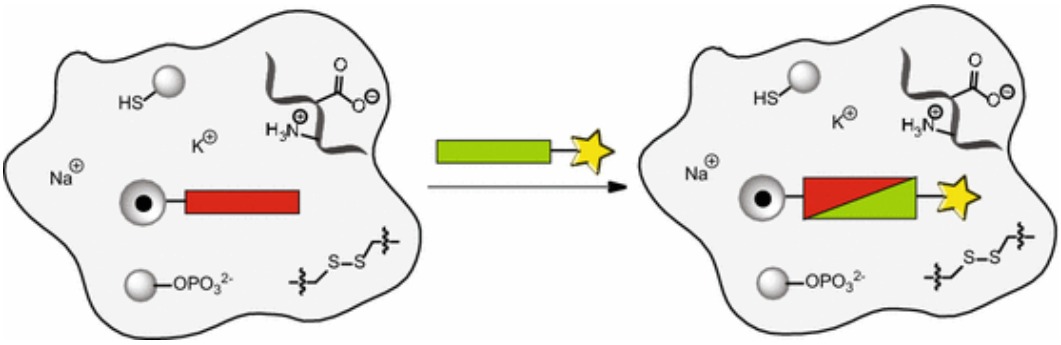

Figure 3: A schematic representation of a bioorthogonal reaction. The green and red rectangles, representing bioorthogonal functional groups, react together in a cellular environment to give a single product.

One of the most prominent bioorthogonal reactions is the inverse electron demand Diels-Alder reaction (iEDDA) between a 1,2,4,5-tetrazine (Tz) and a strained dienophile such as *trans*-cyclooctene (TCO).[11] In the course of the reaction, the highly strained bicyclic species rapidly denitrogenates to give 4,5-dihydropyridazine. In the final step, prototropic isomerization gives rise to 1,4-dihydropyridazine product (Scheme 1).

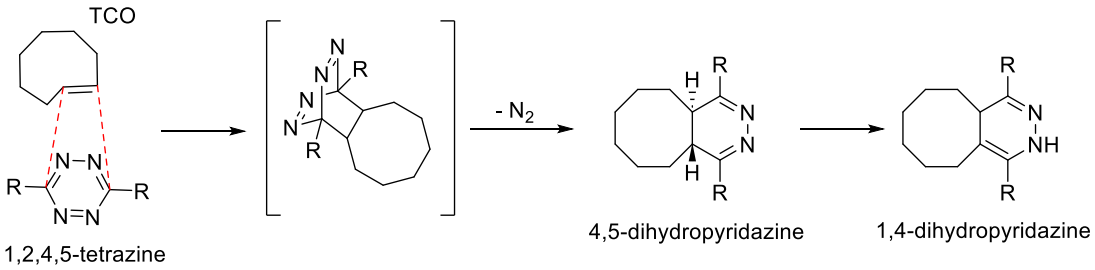

Scheme 1: The bioorthogonal reaction of TCO with Tz.

Next to their ability to participate in bioorthogonal reactions, tetrazines may serve as fluorescence quenching groups. This unique property was first shown by Devaraj *et al.* in 2010,[12] where a series of tetrazine-BODIPY conjugates connected by a flexible (non-conjugated) linker was prepared showing quenching abilities of tetrazines as well as fluorescence turn-on upon reaction by TCO. The fluorescence turn-on values, however, were rather low (up to 20-fold) and a subsequent study showed that these values are much higher

when tetrazine is connected via a conjugated linker to the π-system of the dye (up to 1600-fold).[13] Nevertheless, compounds with such large conjugated π-systems tend to pose other difficulties, mainly coming from complex synthesis, extremely low solubility, and difficulty of isolation from reaction mixtures.[14]

1.3 Tetrazine-mediated fluorescence quenching

In recent years, fluorogenic probes incorporating tetrazine groups have become widely used in biological and medical applications. Their growing popularity is attributed to their outstanding chemoselectivity, fast reaction kinetics, excellent biocompatibility, and adaptable optical properties.[10] Two key challenges in designing new probes is the unknown fluorescence-quenching mechanism in the precursors prior to the bioorthogonal reaction and the fact that achieving fluorescence in the deep-red and near-infrared (NIR) regions while preserving high fluorescence enhancement (FE) ratios remains a significant challenge.[15]

Tetrazine-based probes are most commonly categorized by the mode of connection between the tetrazine and the fluorophore. The first approach is the use of flexible linker – a non-conjugated spacer separating the two systems, maintaining their original electronic properties. One possibility is to use a longer linker that connects the dye to the tetrazine *via* an amide bond (Figure 4A left). Shorter linkage may be achieved by employing an orthogonal phenyl ring separating the two systems (Figure 4A center). In 2021, Wombacher *et al.*[16] introduced a third option, where a linker is used in such a way that tetrazine and the fluorophore are fixed in a face-to-face manner, which shortens the distance between the two and therefore enhances the quenching effect of the tetrazine (Figure 4A right).

The second approach is the use of a conjugated linker, or a single bond connection between the two systems (Figure 4B). The properties of the spacers may vary significantly, which results in various quenching efficiencies and mechanisms.

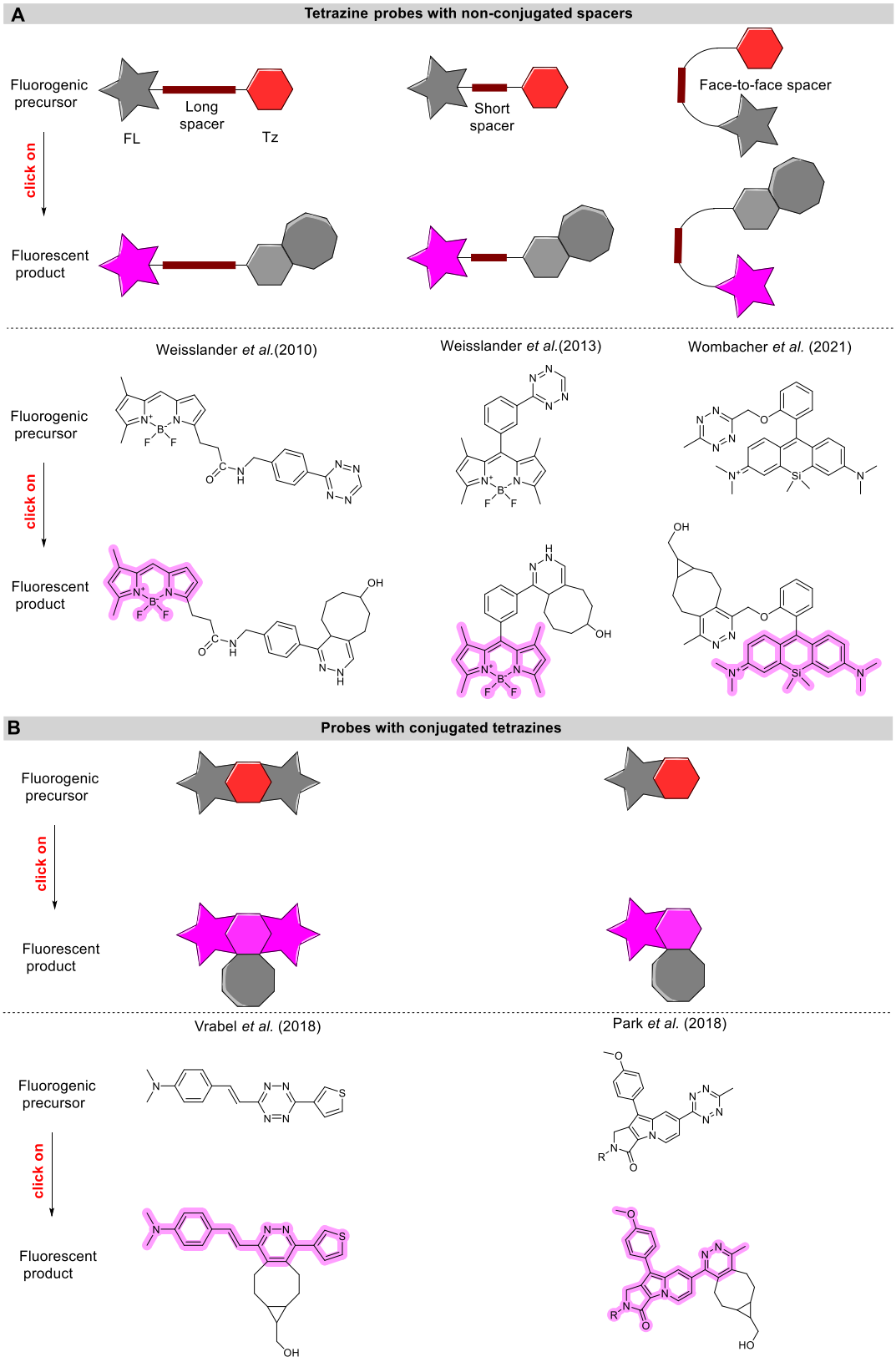

Figure 4: Types of spacers used in the development of fluorogenic probes. Tz = tetrazine, FL = fluorophore.

The quenching mechanism of tetrazines is widely considered to be through energy transfer (EnT). This means that the energy absorbed by the primary fluorophore (donor) is transferred to the tetrazine (acceptor) through EnT, leading to fluorescence quenching via non-radiative decay processes.

In 2021, Choi *et al*. outlined the potential mechanisms of energy transfer (EnT) involved in tetrazine-mediated fluorescence quenching, identifying three main modes[17]: Förster resonance energy transfer (FRET)[18], Dexter energy transfer (DET)[19], and through-bond energy transfer (TBET)[20]. The first mechanism, FRET, is a form of EnT where the energy is transferred *via* coulombic interactions (Figure 5A left). This process requires a substantial spectral overlap between the emission of the fluorophore and the absorption of tetrazine (usually around 520 nm). FRET is also highly dependent on the distance between the donor and acceptor, decreasing with sixth-power dependence. This mechanism is most effective when the donor and acceptor are 10 to 100 Å apart. On the other hand, DET relies on direct electronic interactions (Figure 5A right) requiring the donor-acceptor distance to be even lower (bellow 10 Å). Fluorogenic probes utilizing the mechanisms of FRET and DET are usually the ones containing a non-conjugated, flexible linker, where the linker may adopt various conformations and give rise to the corresponding quenching mechanism. The third mechanism, TBET, is a quenching mechanism most found in probes containing a conjugated linker (Figure 5B). The EnT is mediated directly through the conjugated system, which increases the quenching substantially compared to FRET/DET.[21] As clear as the difference between FRET/DET and TBET may seem, finding out which mechanisms are employed in specific probes remains experimentally challenging.

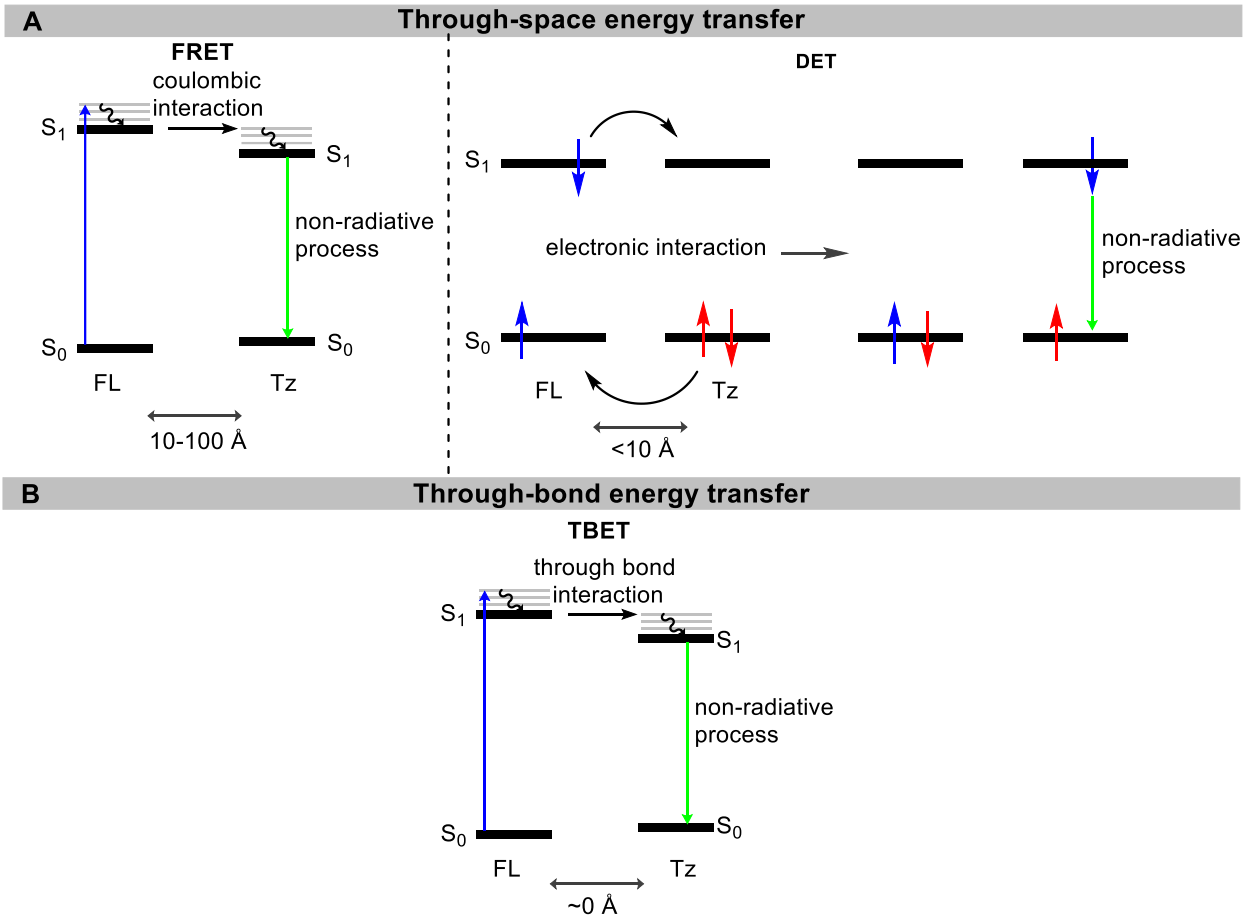

Figure 5: A schematic representation of EnT (A) through space energy transfer quenching mechanisms FRET and DET and (B) through-bond energy transfer (TBET).

For the purpose of unifying quenching mechanism of tetrazine-based fluorogenic probes containing a non-conjugated linker, Liu *et al.* (2021) proposed a mechanism coined energy transfer to a dark state (ETDS).[22] The term "dark state" refers to the S_1 state of tetrazine, which is characterized by a forbidden n→π* transition. This electronic state's properties are described to be primarily responsible for the fluorescence quenching. Two years later, the same group published a study describing a unified quenching mechanism for probes directly conjugated to tetrazines – internal conversion to a dark state (ICDS).[23] The physicochemical description of these processes is beyond the scope of this thesis, however, a notable outcome of the quantum chemical calculations is that EnT and internal conversion (IC) are key quenching forces in the visible region, while in the deep-red and NIR region,

photoinduced electron transfer (PeT, Figure 6) and other mechanisms become predominant.[24]

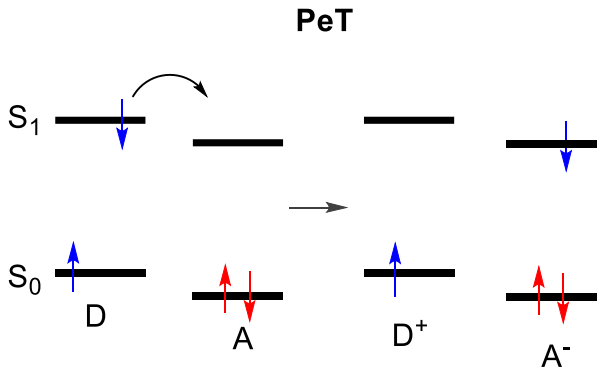

Figure 6: Schematic representation of PeT. D = donor (fluorophore) A = acceptor (quencher).

1.4 Mechanism of fluorescence unquenching via a bioorthogonal "click" reaction

The classical iEDDA bioorthogonal reaction, a so called “click”, is the reaction of a tetrazine with TCO. However, especially when applied to fluorogenic probes, TCO might not be the ideal reaction partner. In 2020, Pinto-Pacheco *et al.*[25] showed that some products of bioorthogonal reactions still exhibit fluorescence quenching properties. Namely, the product of the iEDDA reaction between TCO and a tetrazine – a 1,4-dihydropyridazine – is capable of quenching fluorescence *via* mostly FRET or PeT both intra- and inter-molecularly as demonstrated in multiple experiments. This is especially problematic in red-shifted probes which have the S_1 energy level bellow that of tetrazine and the ETDS does not have a strong quenching effect. This, in cooperation with dihydropyridazine quenching, renders many potentially promising probes useless.[26] Luckily enough, TCO is not the only known bioorthogonal counterpart to tetrazine. For example endo-bicyclo[6.1.0]non-4-yn-9-ylmethanol (BCN)[27] and the spiro[2.3]hex-1-ene (Sph) motif[26] are species that had been shown to yield great results in bioorthogonal applications. BCN reacts with tetrazine in iEDDA forming an aromatic pyridazine ring (Scheme 2). This product does not seem to be involved in fluorescence quenching and the fluorescence enhancement of these reactions

is substantially increased.[25] For this reason, BCN is often used preferentially instead of TCO in fluorogenic probe activation.

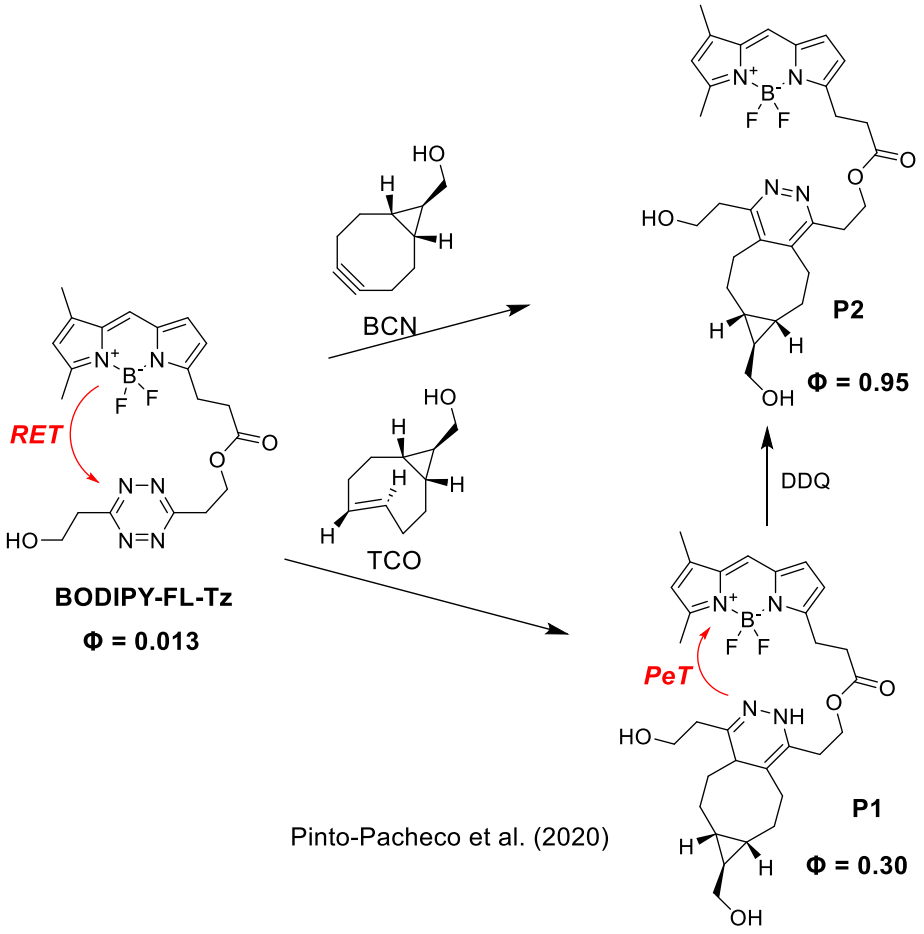

Scheme 2: Activation of tetrazine-containing fluorogenic probe by BCN and TCO via a "click" reaction.

As exemplified by Pinto-Pacheco *et al.*[25], the reaction of BODIPY FL-Tz, proposedly being quenched by resonance energy transfer (RET) mechanism, with BCN gives directly an aromatic product **P2** with great FE ratio, while the reaction with TCO gives the dihydropyridazine product which shows rather low quantum yield and therefore low fluorescence enhancement ratio (Scheme 2).[25] Oxidation of **P1** by addition of 2,3-Dichloro-5,6-dicyano-1,4-benzoquinone (DDQ) gave rise to species **P2** and showed the same spectrochemical characteristics as the product of reaction with BCN.

1.5 Design of red-shifted fluorescent dyes

The drawback of many commercially available fluorescent dyes is that they absorb in the ultraviolet region of the optical spectrum. UV light has limited tissue penetration, it is also cytotoxic and therefore limited to study of cells and tissue slices. For *in vivo* experiments, the ideal wavelength range is ~600-1000 nm – the biological window – where the light transmittance of tissues is highest.[28] Most commonly, the shift toward higher wavelengths is done through extension of π-conjugation, although this methodology might negatively influence other photophysical properties of the studied fluorophores such as quantum yields, fluorescence enhancement etc.[29] However, extension of the conjugated system might not be an attractive option in all cases. Large conjugated systems often exhibit poor solubility, which can restrict their applicability in biological experiments. A notable alternative approach is applied in Si-rhodamine. The red shifting, compared to classical rhodamines (bearing oxygen instead of silicon), is achieved by the conjugation of the σ^* orbitals of silicon and π^* orbital of the chromophore (Figure 7).[30] This, however, is a rather unique example and most of the research is focused on a careful extension of the conjugated systems.

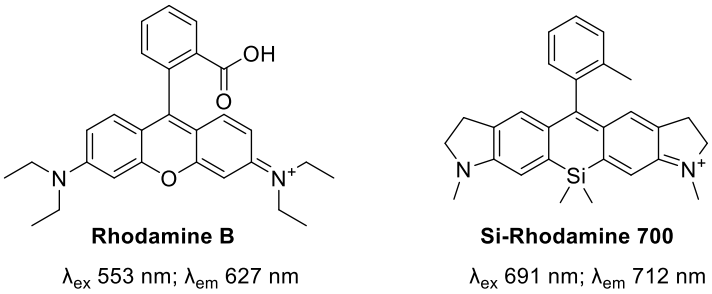

Figure 7: Photophysical properties of **Rhodamine B**[31] and **Si-Rhodamine 700**.[32]

1.6 BODIPY – a versatile, synthetically available fluorophore

BODIPY belongs to a family of one of the most commonly used dyes in modern research. They show great photostability, high fluorescence quantum yield, good solubility, chemical robustness and many other aspects expected for a good fluorophore.[33] Also, the synthetic availability is a prominent feature of BODIPY dyes. If one aims to produce a number of derivatives for a study, purchasing grams of often very expensive precursors[34,35] becomes

unattainable. Additionally, many published preparations of red-shifted bioorthogonally active dyes rely on long syntheses yielding a single product.[12,16] The purpose of this work is to prepare a fluorescent building block that can be derivatized in a robust, simple way in order to get a library of fluorogenic BODIPY probes. In 2017, Katoh *et al.*[36] introduced a novel and robust synthetic pathway for obtaining **BODIPY-FL** in just five steps (Scheme 3).

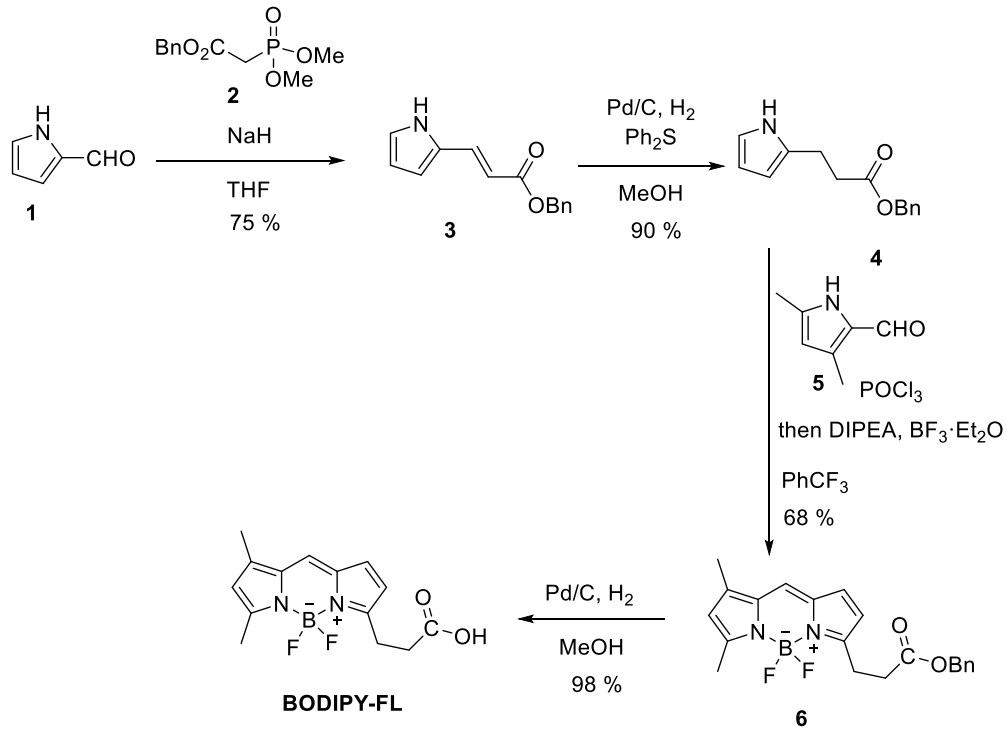

Scheme 3: Synthesis of **BODIPY-FL**.

BODIPY-FL is an attractive starting point for the synthesis of fluorogenic probes, because it carries two distinguished readily available spots for derivatization: one is the carboxylic acid mostly used for amidic coupling with amines, and the second is the methyl-iminium moiety suitable for Knoevenagel-type condensations (Scheme 4). The versatility and synthetic availability of **BODIPY-FL** makes it a very attractive molecule as a starting point for synthesis of novel fluorogenic dyes.

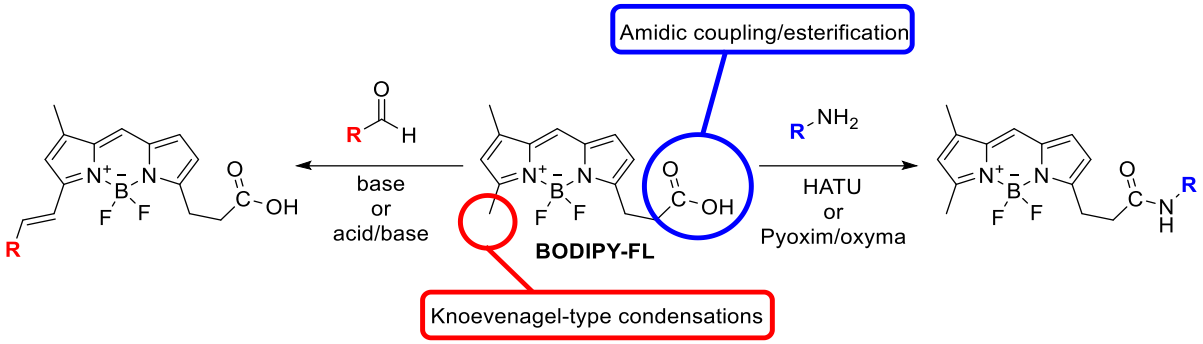

Scheme 4: Derivatization of **BODIPY-FL**.

1.7 Triazinium salts – superior bioorthogonal reagents?

As bioorthogonal chemistry abruptly found its place as one of the indispensable tools of modern chemical biology[37], bioimaging[9], and many other scientific fields, a lot of research has been done with the objective to fine-tune the reaction partners.[15,22,26] Several dienophiles, such as TCO, BCN, and Sph, are commonly used in the iEDDA reaction, as discussed in previous chapters. However, tetrazines have consistently served as the universal diene for more than a decade. In 2015, Kamber *et al.* introduced 1,2,4-triazines as versatile bioorthogonal reagents.[38] They react in a similar fashion as tetrazines, however, the iEDDA dihydropyridine product undergoes a spontaneous oxidation, giving rise to a pyridine (Scheme 5). They were prepared mostly in effort to fight a fundamental limitation of tetrazines – their instability, particularly in the presence of nucleophiles.[39]

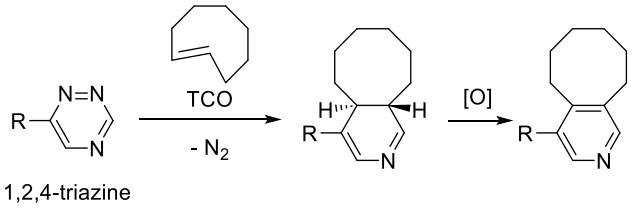

Scheme 5: The iEDDA reaction between a 1,2,4-triazine and TCO.

The improved stability unfortunately also caused lower reactivity of triazines towards their bioorthogonal counterparts. In 2023, our group presented another alternative to tetrazines – triazinium salts (Trz^+).[40] These charged species combine the best of both worlds – great stability and reactivity. Surprisingly, triazinium salts containing a bulky *t*Bu group on the charged nitrogen were found to be most reactive, which was attributed either to increased

hydrophobicity effect, or enhanced dispersion forces. The mechanism of the triazinium iEDDA reaction is similar to that of tetrazines, but hydrolysis of the N-alkyl must proceed in the course of the reaction to give N_2, alkyl-OH and the "click" product (Scheme 6). Two possible mechanisms for the "click" reaction have been suggested: either departure of diazonium species in the retro-DA step followed by hydrolysis to generate the alkyl-alcohol and N_2 (Scheme 6 Path A), or the hydrolysis precedes the retro-DA step and the subsequent denitrogenation happens in a similar fashion to standard tetrazine iEDDA reaction (Scheme 6 Path B). The presence of the alkyl-alcohol was confirmed by NMR spectroscopy. A limitation of triaziniums is that they only show good results with BCN, leaving TCO-based reagents out of the picture.

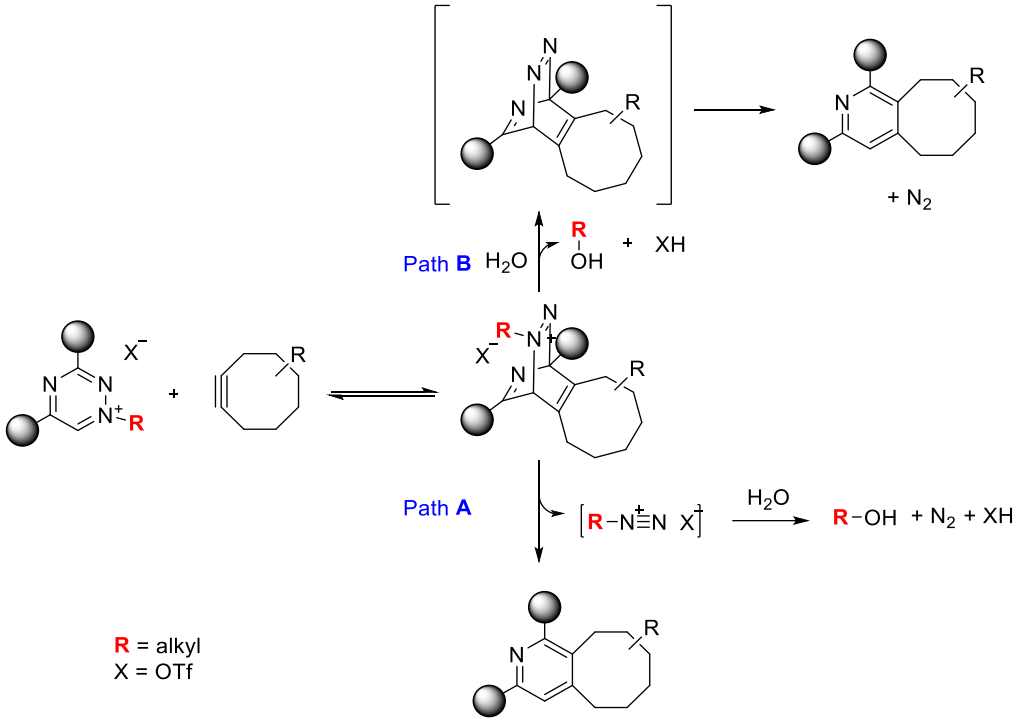

Scheme 6: Mechanism of Trz^+ iEDDA.

In a subsequent study, our group showed the fluorogenic properties of Trz^+-coumarin derivatives, highlighting the fluorescence quenching properties of these new bioorthogonal reagents.[41]

Furthermore, in 2025, our group published a detailed study of triazinium quenching mechanism for probes with flexible non-conjugated linkers along with demonstration of their use in various experimental set-ups, such as imaging of small molecules (organelle targeted probes and drugs),

cell surface antigens, HaloTag fusion proteins, proteins containing artificial amino acids, and metabolically engineered glycoconjugates.[42]

Typically, the relative quenching efficiency increases with greater spectral overlap between the emission spectrum of the fluorophore and the absorption spectrum of the quencher. Tetrazines have weak absorption maximum at around 520 nm (ε_{max} = 180 M^{-1} cm^{-1}), which makes them good quenchers only for fluorophores having similar excited state energies, mostly those in green spectral region (such as BODIPY). On the other hand, triaziniums exhibit significantly stronger panchromatic absorption (ε_{max} = 18000 M^{-1} cm^{-1}), which makes them efficient quenchers in virtually any fluorophores in the 450–650 nm spectral range. A limitation of triaziniums is that the Trz^{+}BCN adducts retain absorption in the visible region (compared to tetrazines giving colorless TzBCN adducts) and fluorescence therefore cannot be fully restored. Detailed computational studies clarified the quenching mechanism of triazinium-based fluorogenic probes: (a) triaziniums have a tendency to form stacked conformations with fluorophores, substantially decreasing their spatial distance, and resulting in static fluorescence quenching (Figure 6A) (b) photoinduced electron transfer (PeT) resulting from electron poor nature of triaziniums (susceptibility to reduction), which can suppress fluorescence of a vast range of fluorophores. PeT is made possible thanks to negatively shifted reduction potentials of fluorophores in the excited state. Also, density functional theory (DFT) calculations revealed that triazinium quencher has approximately 0.2 V higher reduction potential than tetrazine quencher, which makes triazinium more susceptible to reduction and, therefore, PeT-based fluorescence quenching (Figure 6B) and (c) the strong panchromatic absorption enables spectral overlap with fluorophores and thus enables efficient quenching (Figure 6C).[42]

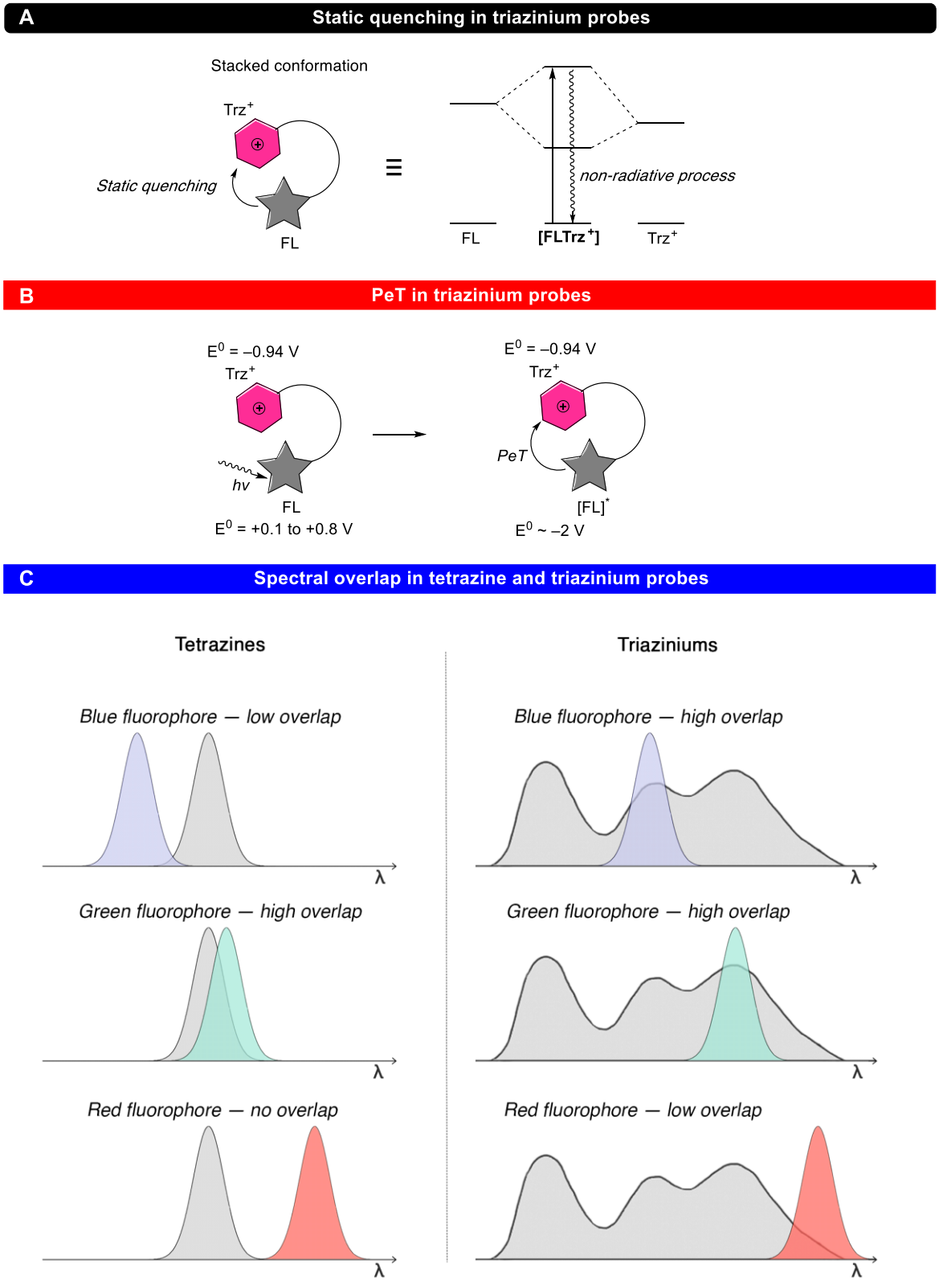

Figure 8: Fluorescence quenching mechanism of triaziniums: (A) static quenching (B) PeT mediated quenching and (C) spectral overlap with fluorophores and comparison with tetrazines.

2. Aims and objectives

The purpose of this thesis is to design, prepare, and test new red-shifted fluorogenic probes of general structure **A** or **B** for bioimaging applications. Workflow to get compound type **A** may be summarized as follows:

a) Synthesis of **BODIPY-FL**
b) Utilization of Knoevenagel condensation in order to achieve extended conjugation and desired red-shift (blue sphere)
c) Selection of best candidates for further derivatization
d) Derivatization of best candidates with a tetrazine or a triazinium *via* amidic coupling on carboxyl group (red hexagon)
e) Spectrofluorometric measurements of final compounds
f) Live-cell experiments with selected candidates

In compound B, a tetrazine moiety (red hexagon) is introduced via a Knoevenagel condensation, and further derivatization of the carboxylic acid (green sphere) can be applied to enhance solubility or other properties. This modification leads to compound type **C**, especially if the original properties of **B** present challenges in experimental applications.

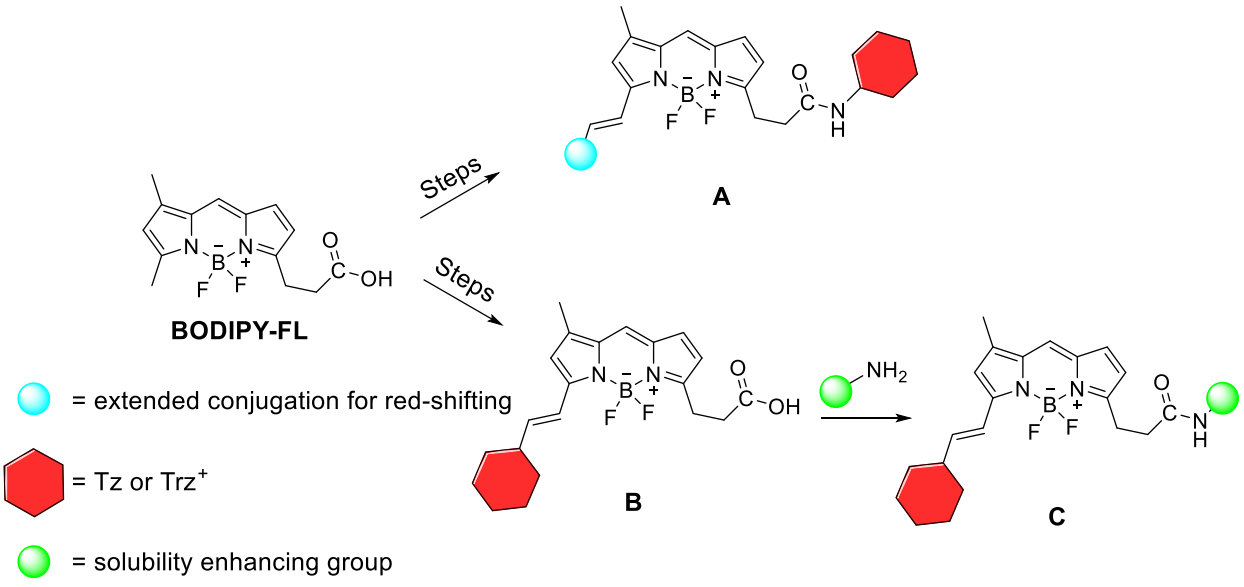

3. Results and discussion

3.1 Synthesis of **BODIPY-FL**

BODIPY-FL was chosen as the building block for further derivatization due to its synthetic availability and versatility. The synthesis of **BODIPY-FL** was performed as was described by Katoh *et al.* (Scheme 7).[43] First step of the synthesis is the Horner-Wadsworth-Emmons (HWE) reaction between the pyrrole **1** and phosphonate **2** to give the α,β-unsaturated ester **3**. Then, selective reduction of the double bond was achieved by employing Ph_2S as a catalyst poison (due to presence of benzyl ester) to give **4**. Reaction with 3,5-dimethyl-pyrrole-2-carboxaldehyde **5** followed by complexation with $BF_3{\cdot}Et_2O$ afforded compound **6**. Subsequent reductive benzyl deprotection gave **BODIPY-FL**.

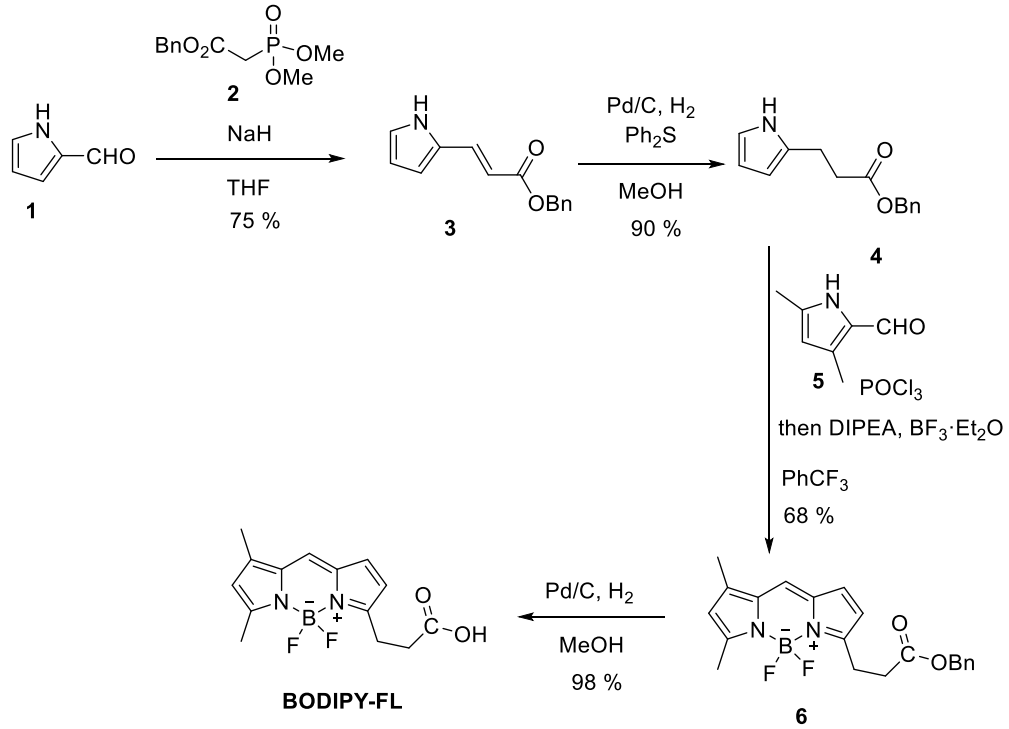

Scheme 7: Synthesis of **BODIPY FL**.

The phosphonate **2** for HWE reaction was prepared according to previously published procedure (Scheme 8):[44]

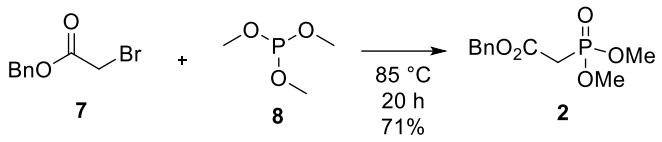

Scheme 8: Synthesis of **2** as a reagent for HWE reaction.

3.2 Strategies for **BODIPY-FL** derivatization

As discussed in the previous chapters, **BODIPY-FL** contains two main sites for derivatization: carboxylic acid and methyl-iminium moiety (Scheme 9). Knoevenagel condensation (Scheme 9A) in the methyl-iminium position allows derivatization of BODIPY by the introduction of the directly conjugated **R** moiety. This reaction presents multiple possibilities – either a simple conjugation extension is done in order to achieve red-shift, or a tetrazine/triazinium moiety may be introduced, possibly providing both red-shift and fluorescence quenching.

Amidic coupling is a simple and high-yielding reaction that can be used to introduce a variety of functionalities bearing amine group. This site may be used to attach tetrazine or a triazinium *via* non-conjugated flexible linker, or, if tetrazine or a triazinium were introduced in the Knoevenagel step, this site could be used to improve physicochemical properties of the potentially highly insoluble BODIPY derivatives.

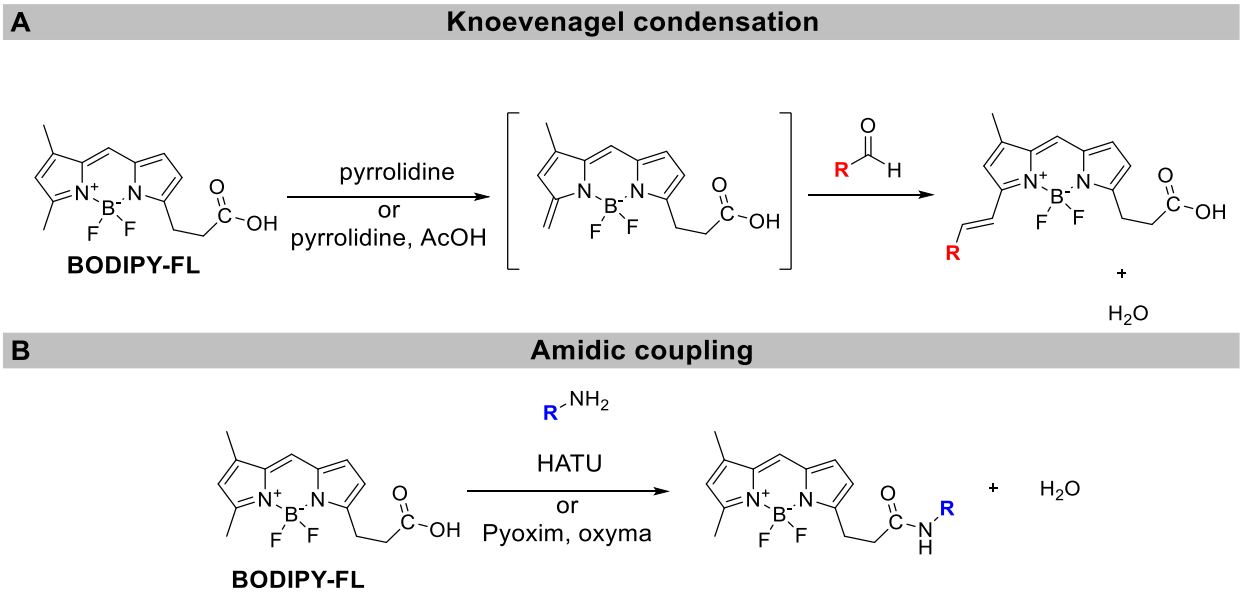

Scheme 9: BODIPY FL derivatization.

3.3 Red-shifting of **BODIPY-FL** using Knoevenagel condensation

In order to identify good candidates for next synthetic steps, **BODIPY-FL** was subjected to Knoevenagel condensation with a library of unsaturated aldehydes in order to achieve extended conjugation and desired red-shift (Scheme 10). The results are summarized in Table 1.

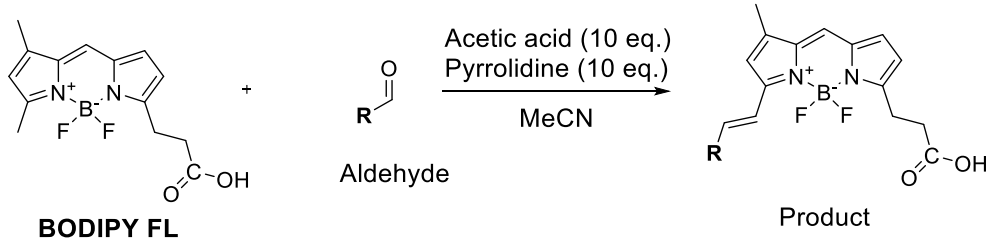

Scheme 10: A general Knoevenagel condensation between **BODIPY-FL** and an aldehyde.

The value of absorption maxima was not the only characteristic taken into account in the selection process. Some of the reactions provided very little product according to LCMS and they were not taken into consideration (data not shown). Also, entries 19-21 were found to be greatly red-shifted, but they also have fluorescence quenched. Since fluorescence quenching is supposed to be mediated by a bioorthogonally reactive group (for the purpose of this work) in order for the compounds to be fluorogenic, these compounds were also discarded.

Table 1: Absorption maxima of Knoevenagel condensation products following reaction shown in Scheme 10. [a]Absorption maxima of products were found using LCMS. [b]Selected candidates are highlighted in green color.

Entry	Aldehyde	Absorption maximum of product (nm)[a]	Entry	Aldehyde	Absorption maximum of product (nm)[a]
1	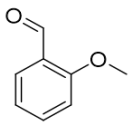	572	12	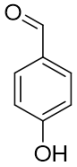	567
2	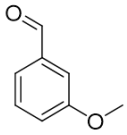	566	13	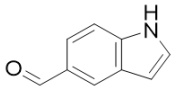	573
3	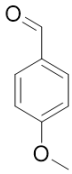	569	**14**[b]	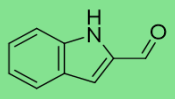	**590**
4	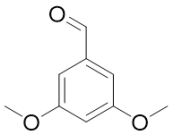	567	15	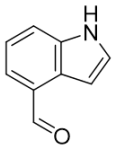	580
5	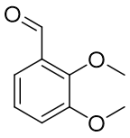	569	16	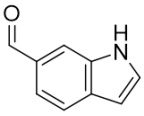	590
6[b]	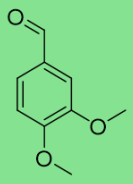	**579**	17	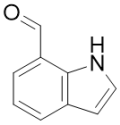	578

7	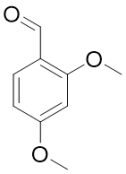	580	18	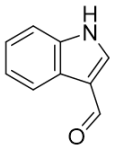	580
8	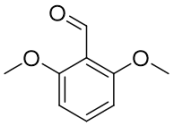	574	19	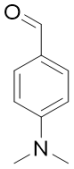	607
9	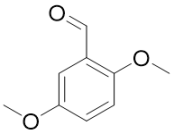	574	20	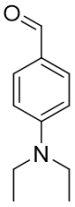	614
10	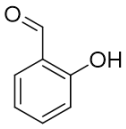	565	21	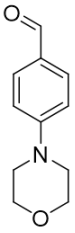	593
11	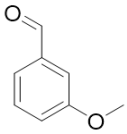	560			

The two most promising derivatives **10** and **12** were prepared in larger scale (Scheme 11) by using the aldehydes as described in Table 1 (entries 6 and 14). **BODIPY-FL** was subjected to the reaction with commercially available aldehydes **9** and **11** in the presence of pyrrolidine and acetic acid. These reaction conditions seem to yield the best results, probably due to water not being eliminated when only base (pyrrolidine) and not acetic acid are present. The conversion of the reactions seemed very good on LCMS and TLC, however a lot of compound was lost in the purification process. This is presumably because the compounds have a tendency to stick to both reversed phase (RP) and normal silica, making every column chromatography unpleasant. Using

expensive RP columns for purification of these compounds is therefore disfavored, however usually necessary.

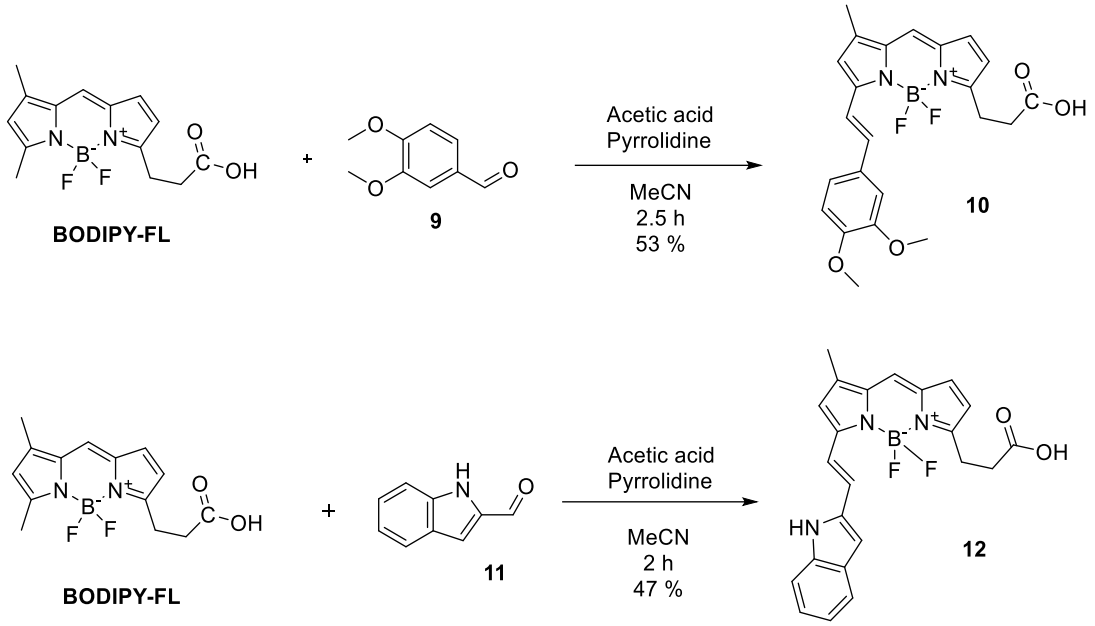

Scheme 11: Synthesis of **10** and **12**.

3.4 Installation of non-conjugated bioorthogonal fluorescence quenching group

Compounds **BODIPY-FL**, **10**, and **12** have a free carboxylic acid moiety that can be further derivatized using amidic coupling. A tetrazine with amino group **15** was prepared according to previously published procedure (Scheme 12).[45] The synthesis starts by the reaction of **13** with MeCN and hydrazine monohydrate in the presence of $Zn(OTf)_2$ as a Lewis acid, followed by oxidation with sodium nitrite and HCl to give **14**. Relatively mild Boc-deprotection conditions gave **15** in a quantitative yield.

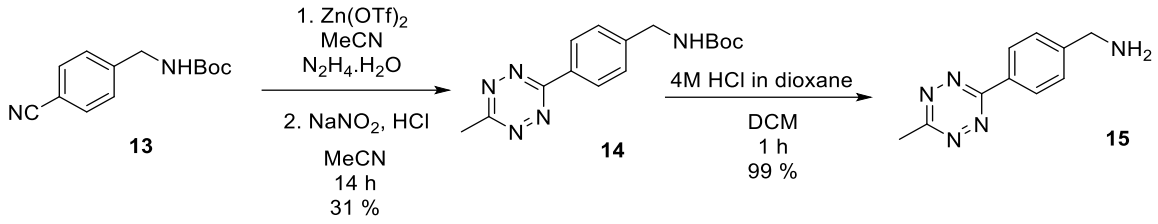

Scheme 12: Synthesis of Tz precursor **15**.

Tetrazine **15** was installed on the BODIPY dyes **BODIPY-FL**, **10**, and **12** to give the compounds **BODIPY-FL-Tz**, **16** and **17**, respectively (Scheme 13). The choice of amidic coupling reagents was based on previously published procedure.[46] The probes **BODIPY-FL-Tz**, **16** and **17** exhibit even lower solubility than their respective precursors and the yields of the reactions are relatively low due to losses during purification.

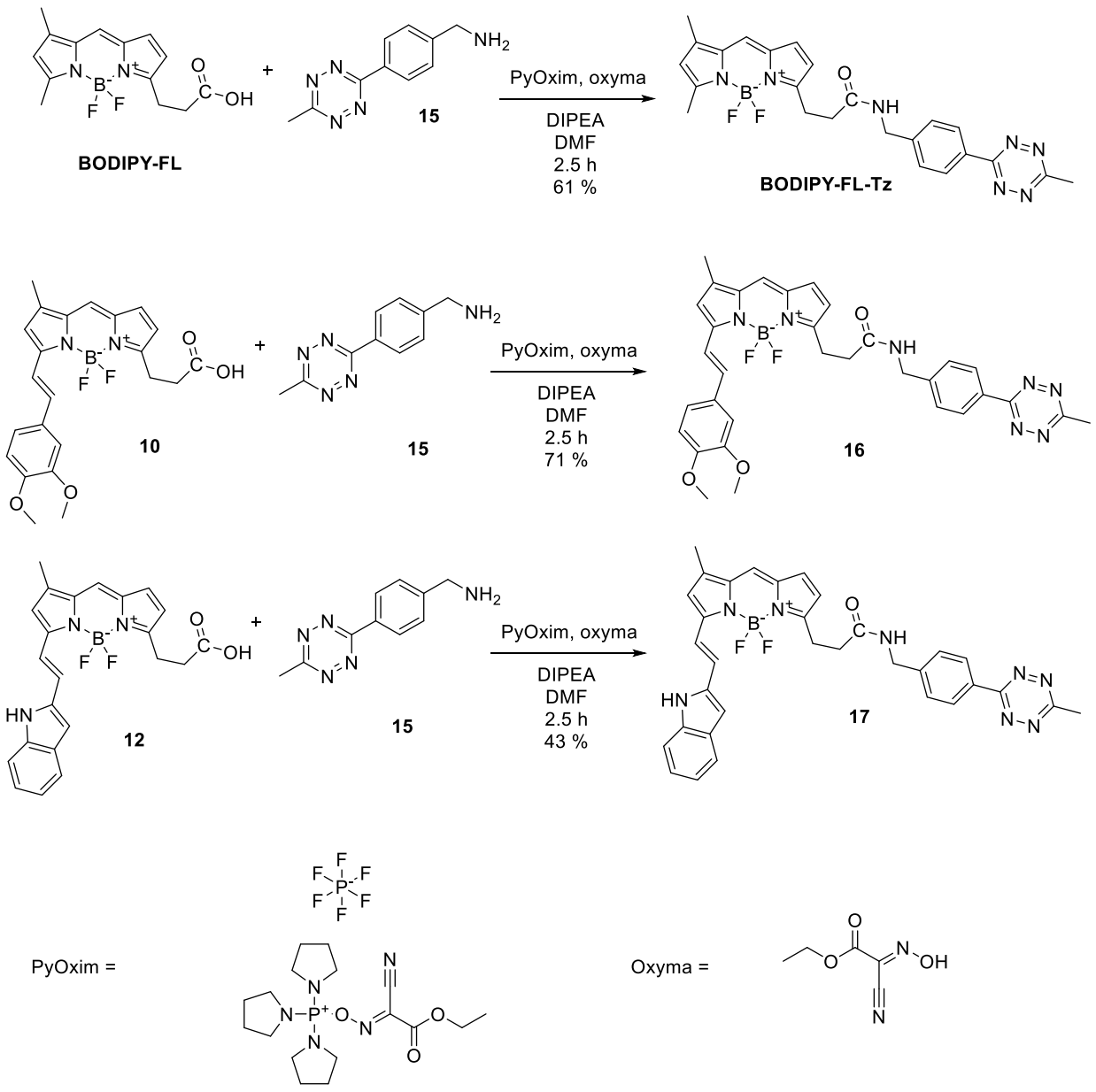

Scheme 13: Preparation of BODIPY-Tz derivatives.

Next, a series of BODIPY-Triazinium (BODIPY-Trz$^+$) derivatives **BODIPY-FL-Trz$^+$**, **19** and **20** was prepared (Scheme 14) with HATU as the coupling reagent. The triazinium **18** used was previously synthesized in our research group. These probes exhibit slightly better solubility in polar solvents (most probably due to presence of positive charge on the triazinium nitrogen), but they seem to eagerly exchange ions or otherwise decompose on silica. Pre-purification on silicagel of the compounds **BODIPY-FL-Trz$^+$**, **19** and **20** was, however, necessary due to presence of insoluble

byproducts, which could clog the column. Then, final purification by RP column chromatography was done with addition of 0.1 % trifluoroacetic acid (TFA) instead of formic acid, because formic acid causes decomposition of the triazinium core.[42]

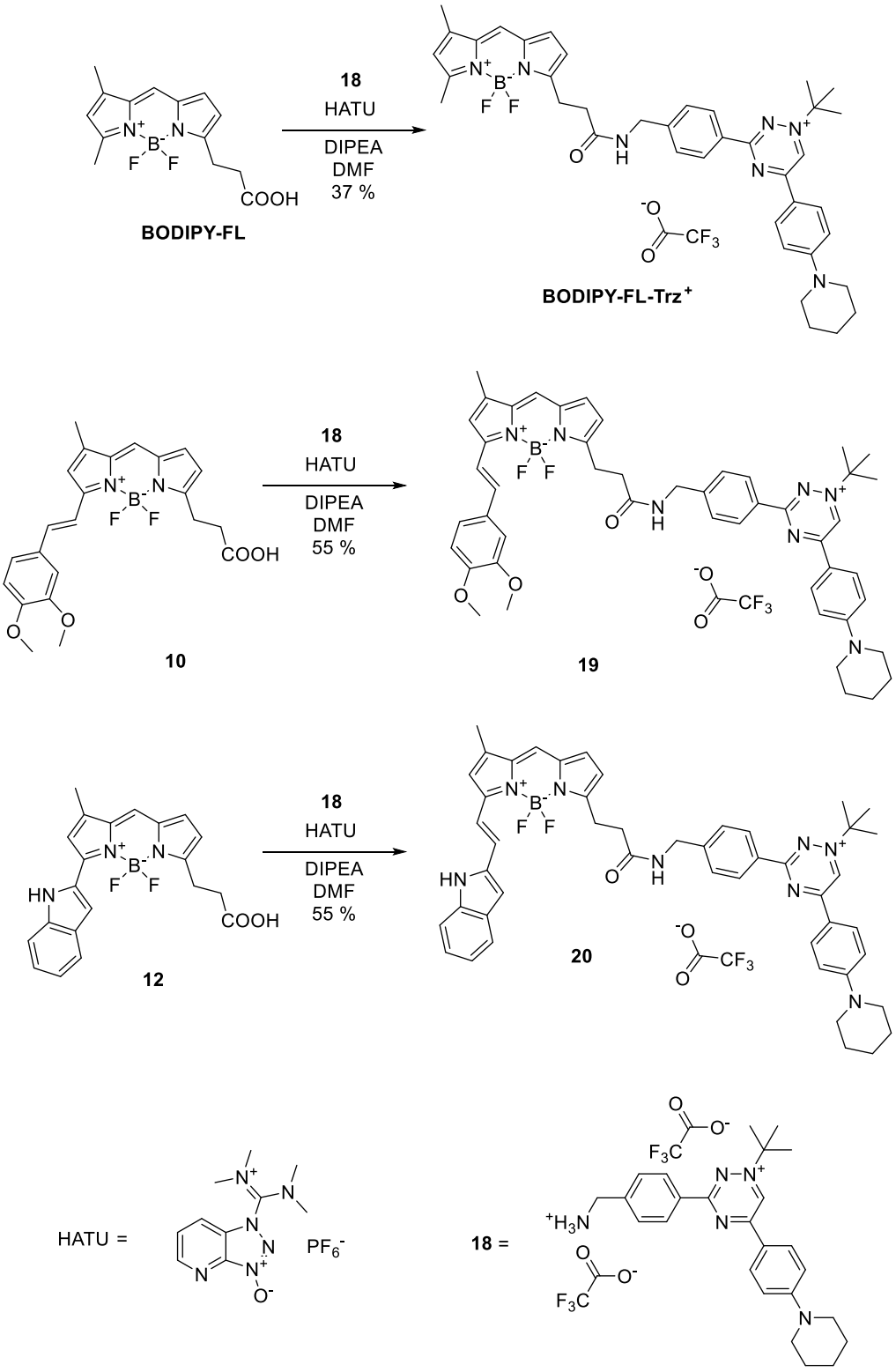

Scheme 14: Preparation of BODIPY-Trz^{+} derivatives.

3.5 Synthesis of conjugated BODIPY-Tetrazine derivative

To further investigate the quenching ability of tetrazine, an additional **BODIPY-FL** derivative was designed. In this case, the tetrazine moiety was directly conjugated to the BODIPY core, providing a counterexample to the previously described probes. The retrosynthetic analysis of the conjugated BODIPY-Tz compound (**24**) is shown in Scheme 15. The probe was designed to bear a similar structural motif on the tetrazine as seen in the non-conjugated probes **BODIPY-FL-Tz**, **16**, and **17**, in order to maintain comparable chemical properties. However, a direct comparison cannot be made due to the different mode of attachment of the tetrazine to the **BODIPY-FL** core.

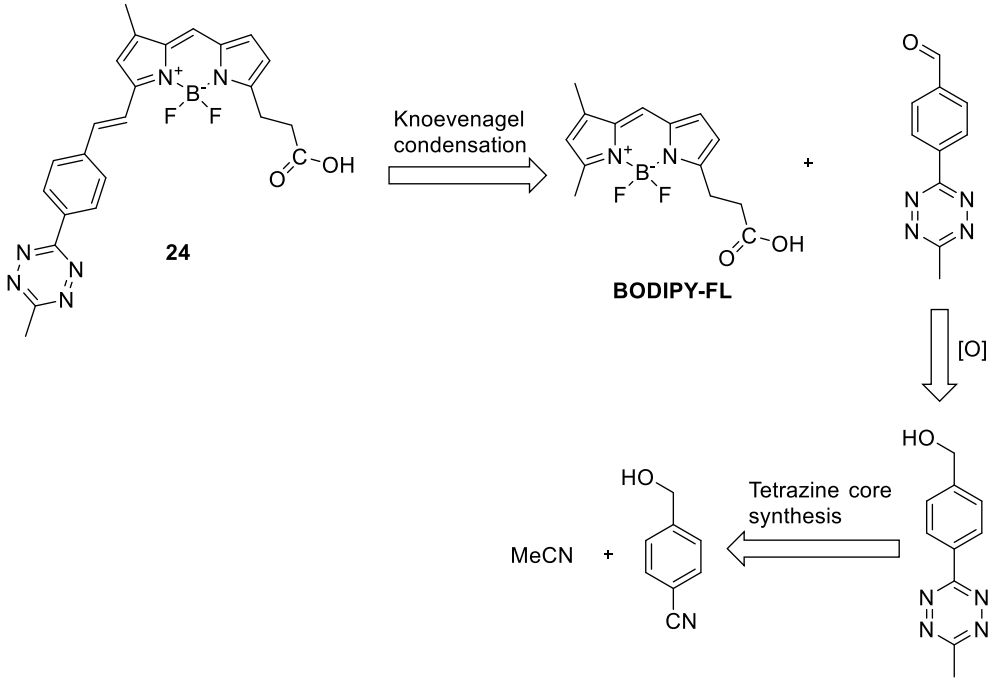

Scheme 15: Retrosynthetic analysis of the conjugated probe **24**.

The tetrazine-aldehyde **23** was prepared according to a previously published procedure.[47] First, the tetrazine core was synthesized from 4-(hydroxymethyl) benzonitrile **21** and MeCN in the presence of hydrazine monohydrate and $Zn(OTf)_2$ as Lewis acid followed by oxidation with $NaNO_2$ and 2M HCl to give compound **22**. The oxidation of compound **22** with Dess-Martin periodinane afforded **23** in an excellent yield (Scheme 16).

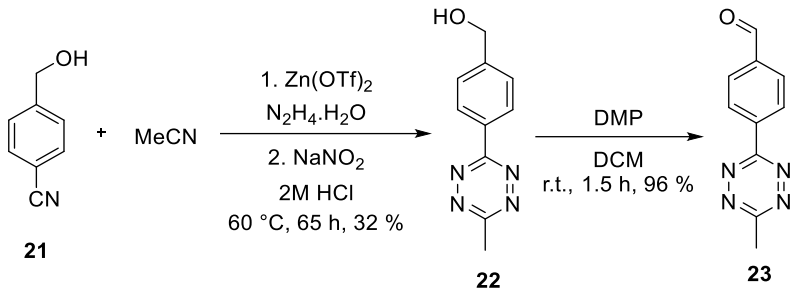

Scheme 16: Synthesis of tetrazine-aldehyde **23**.

Next, Knoevenagel condensation between the tetrazine **23** and **BODIPY-FL** was performed under standard conditions using pyrrolidine and acetic acid in MeCN to give **24** in a 12% yield (Scheme 17).

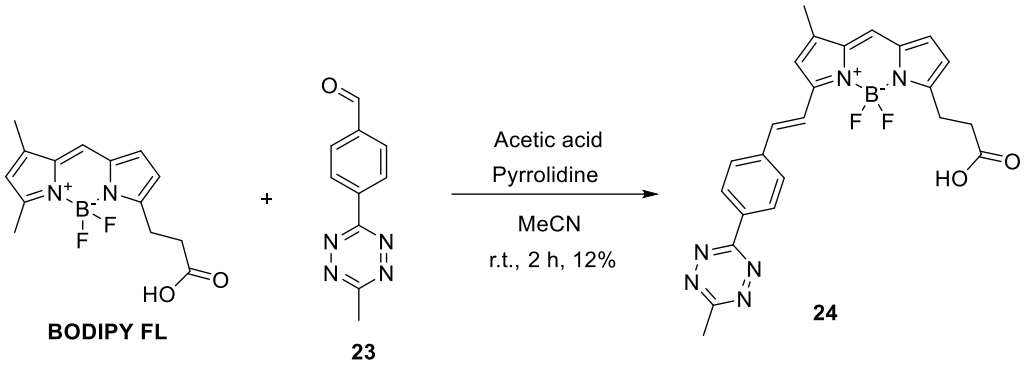

Scheme 17: Synthesis of the fluorogenic probe **24** *via* Knoevenagel condensation.

The low yield is attributed to material losses during the purification process, as the conversion seemed excellent on LCMS. This reaction was repeated several times due to product decomposition on silica. When methanol was used, its addition to one of the double bonds of **24** was observed on LCMS, and also on NMR. In the end, the safest way to obtain **24** was to remove the solvents with a flow of N_2, followed by drying on high vacuum and then loading on reversed phase (RP) column in pure acetonitrile. A large amount of the compound precipitated on the RP column and had to be washed out with DMF, which caused the low yield, but sufficient amount of the compound **24** was isolated to conduct desired experiments.

As it turns out, the compound **24** does not exhibit such low solubility as expected and no further derivatization was necessary for subsequent experiments. The free carboxylic acid represents a highly versatile functional group for derivatization (e.g., via amide coupling), however, no such

derivatives were prepared in the course of this work and their development is left for future studies.

3.6 Spectrofluorometric measurements

3.6.1 Probes containing a non-conjugated quenching moiety

The six final compounds containing a non-conjugated fluorescence quencher **BODIPY-FL-Tz**, **16**, **17**, **BODIPY-FL-Trz$^+$**, **19**, and **20** were tested for their photophysical properties. First, absorption maxima were determined using UV-Vis spectrophotometry. Secondly, spectrofluorometric properties of the parent compounds **BODIPY-FL**, **10**, and **12** were measured in order to obtain useful information for measurements of their fluorogenic counterparts **BODIPY-FL-Tz**, **16**, and **17**, respectively. Then, emission spectra of the compounds were measured before and after their activation by the bioorthogonal counterpart (TCO and BCN).

Compounds **10** and **12** showed a considerable red-shift compared to **BODIPY-FL** (Figure 9). As expected, the achieved red-shift causes lowered fluorescence intensity of the compounds **10** and **12**.

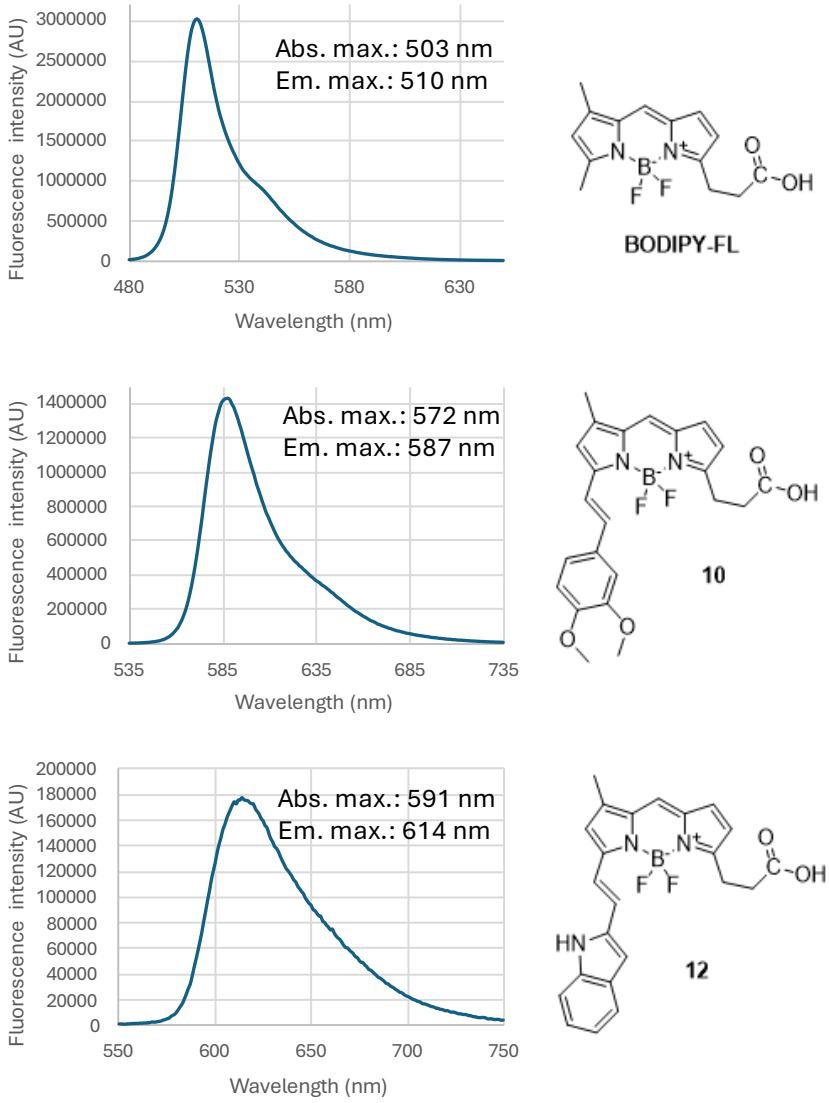

Figure 9: Emission spectra of compounds **BODIPY-FL**, **10**, and **12**. Solvent system: 50% MeCN in H_2O. *c* = 1 µM.

There are several ways to calculate fluorescence turn-on values reported in literature. First is to divide fluorescence intensity of the click product at the emission maximum by the fluorescence intensity of the fluorogenic probe before click. Second approach is to divide the integrated areas of the whole emission spectra. In the third approach, the quantum yields of the probe before and after reaction are divided. The first approach tends to show the highest turn-on values and is the least trustworthy. The other two approaches tend to show comparable results. This was shown in an article published by our research group, which concentrated on the design, synthesis and

characterization of novel triazinium probes.[42] For the purpose of this work, the second method was chosen for the calculation of turn-on values for its good precision and relative ease of application compared to calculating quantum yields.

The experimental workflow involved an initial measurement of the emission spectrum of the respective compound (Figure 10, **1.**), followed by the initiation of kinetic measurements (Figure 10, **2.**). Subsequently, the reactive partner—either TCO or BCN—was added to the solution (Figure 10, **3.**). After an incubation period of approximately 30 minutes, during which the reaction kinetics were measured, the emission spectrum of the resulting solution was recorded to assess the changes in fluorescence following the bioorthogonal reaction (Figure 10, **4.**).

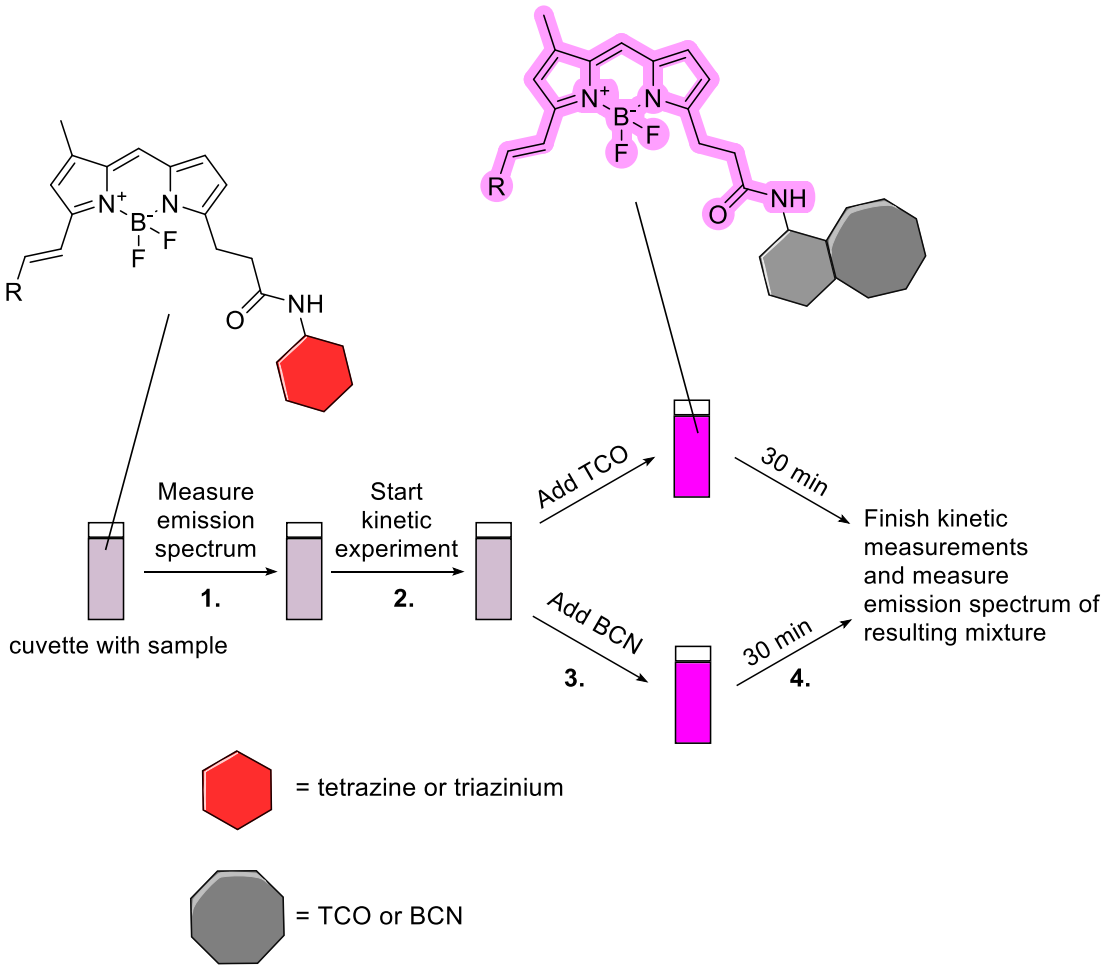

Figure 10: The experimental workflow of spectrofluorometric experiments.

The first series of spectrofluorometric experiments was conducted on the tetrazine probes **BODIPY-FL-Tz**, **16**, and **17** according to the workflow diagram shown in Figure 10. The expected fluorescent products with TCO and BCN are schematically represented in Scheme 18.

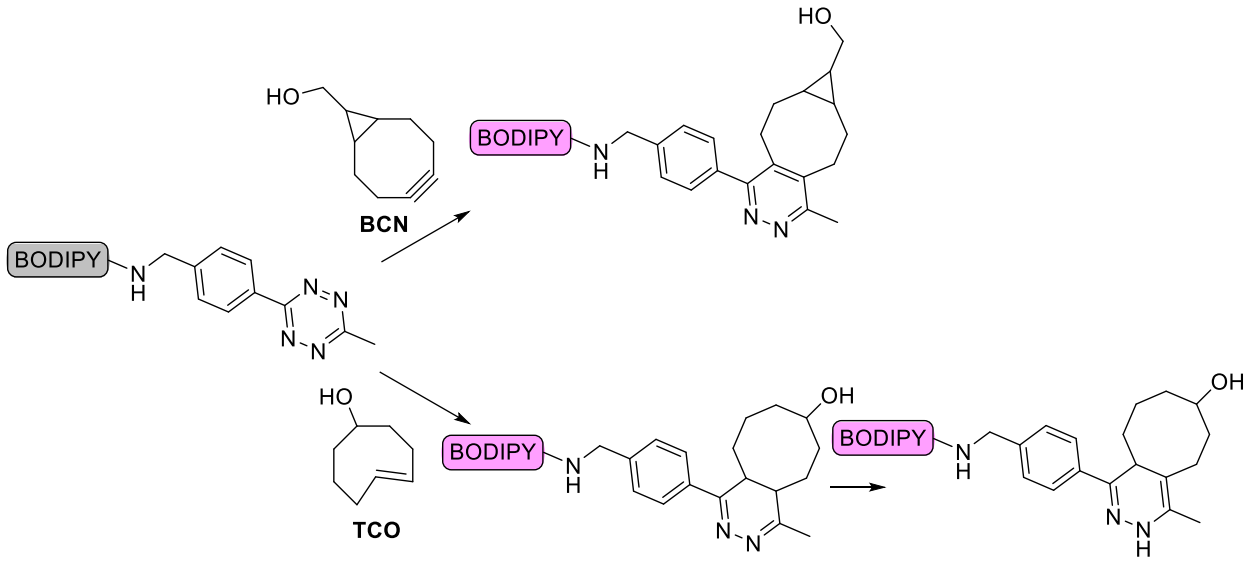

Scheme 18: Fluorescence turn-on of tetrazine probes with TCO and BCN.

Reaction kinetics reveal, that the non-red-shifted **BODIPY-FL-Tz** shows great fluorogenic properties, but the reactivity and the fluorescence enhancement of the red-shifted probes **16** and **17** is rather low (Figure 11).

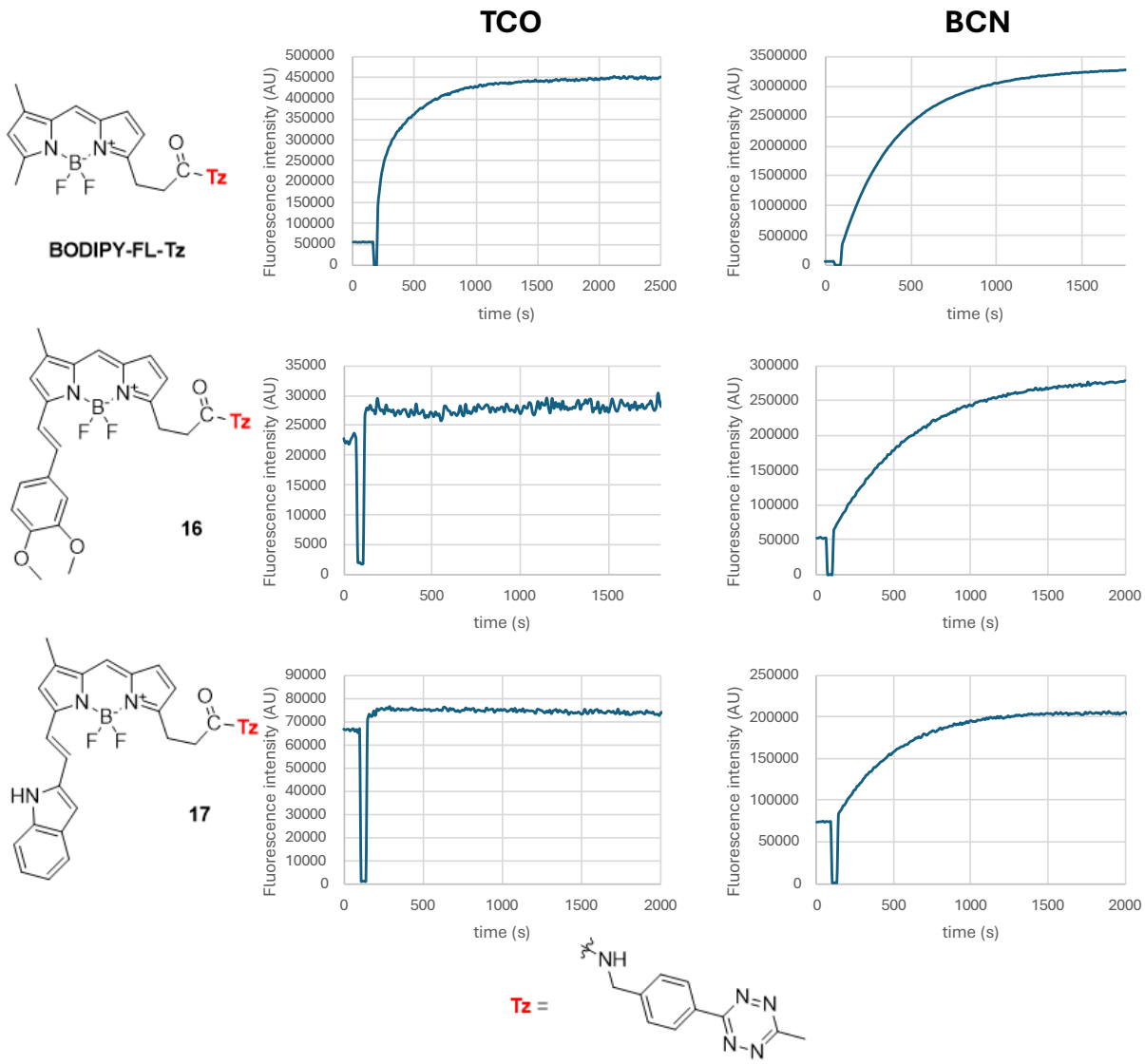

Figure 11: Reaction kinetics of non-conjugated tetrazine probes after addition of 1 µL of 0.5M TCO in MeOH (left) and 1 µL of 0.5M BCN in DMSO (right). Solvent system: 50% MeCN in H_2O. c = 1 µM, V = 1 mL.

Compounds **16** and **17** show a substantial red-shift but their fluorescence turn-on values are relatively low, however slightly better with BCN (4.5, 2.7, respectively) than TCO (1.2, 1.1, respectively) (Table 2 and Figure 12). The better results with BCN than TCO can be attributed to fluorescence quenching properties of the dihydropyridazine product (Scheme 18, Chapter 4.4). The generally low turn-on values are most likely a consequence of the red-shift itself, indicating that tetrazines are not efficient quenchers in this spectral region. This is evident in the results for **BODIPY-FL-Tz** (turn-on (BCN) = 66), which exhibits significantly improved fluorogenic properties (Table 2 and Figure 12).

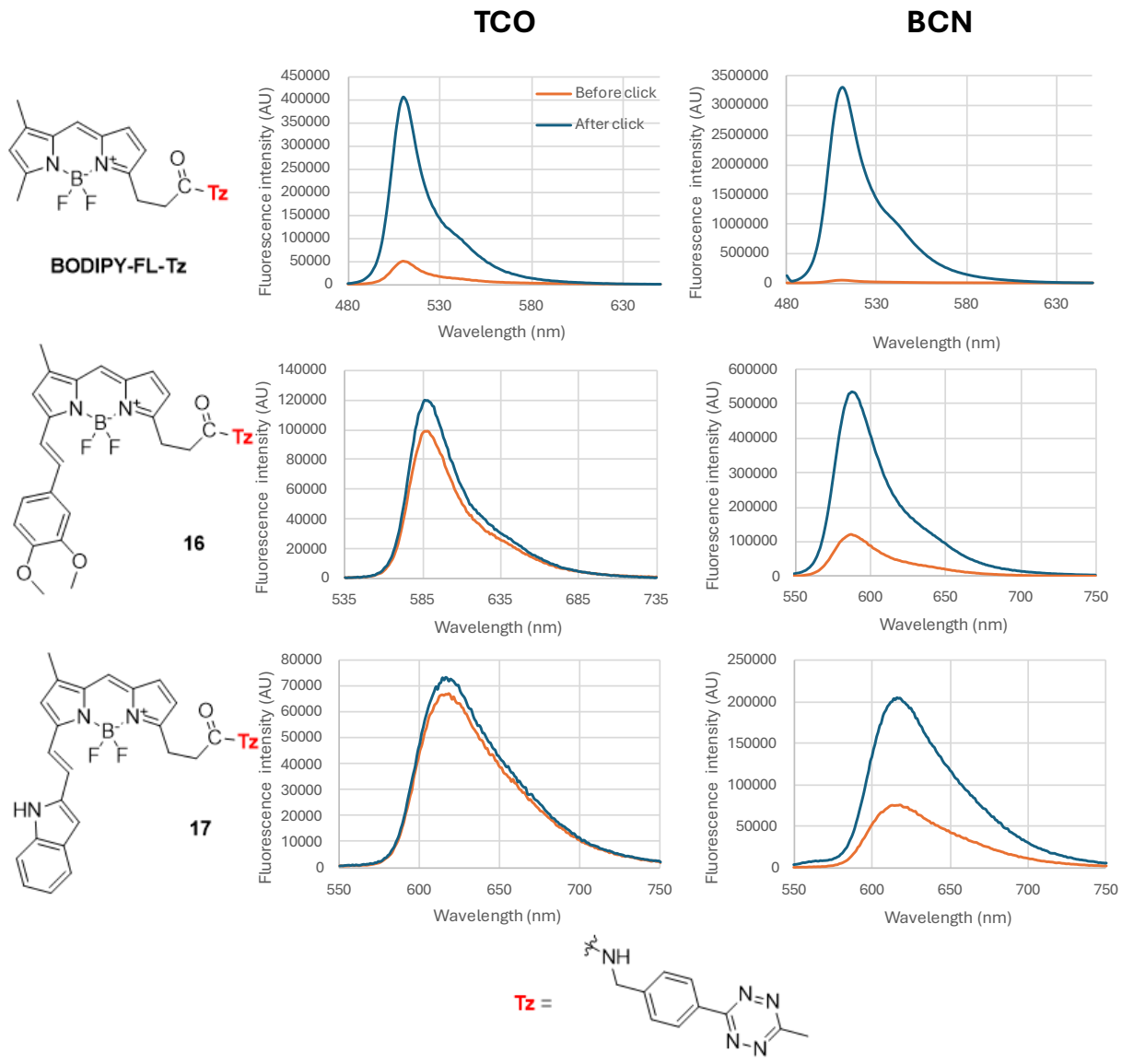

Figure 12: Emission spectra of tetrazine probes. Emission spectra were measured before (orange lines) and after (blue lines) the addition of 1 µL of 0.5M TCO in MeOH (left column) and 1 µL of 0.5M BCN in DMSO (right column), both approximately 30 min after the addition. Solvent system: 50% MeCN in H_2O. c = 1 µM, V = 1 mL.

Table 2: Photophysical properties of the non-conjugated fluorogenic tetrazine probes[a]

Probe	Absorption maximum (nm)	Emission maximum (nm)[b]	Fluorescence turn-on[c]	
			TCO	BCN
BODIPY-FL-Tz	504	510	7.9	66
16	573	586	1.2	4.5
17	593	618	1.1	2.7

[a]Solvent system: 50% MeCN in H_2O. c = 1 µM [b]Emission maxima before "click" reaction. [c]Turn-on calculated by dividing the integrated emission areas.

These results clearly suggest the need for a different quenching strategy when it comes to red-shifted fluorogenic probes.

In order to investigate, whether triaziniums can act as a better fluorescence quenching moiety than tetrazines, the triazinium-containing compounds **BODIPY-FL-Trz$^+$**, **19**, and **20** were investigated for their fluorogenic properties in a similar manner. However, triaziniums are not reactive toward TCO, so only BCN was used in the experiments. The expected products of the reaction with BCN are schematically represented in Scheme 19.

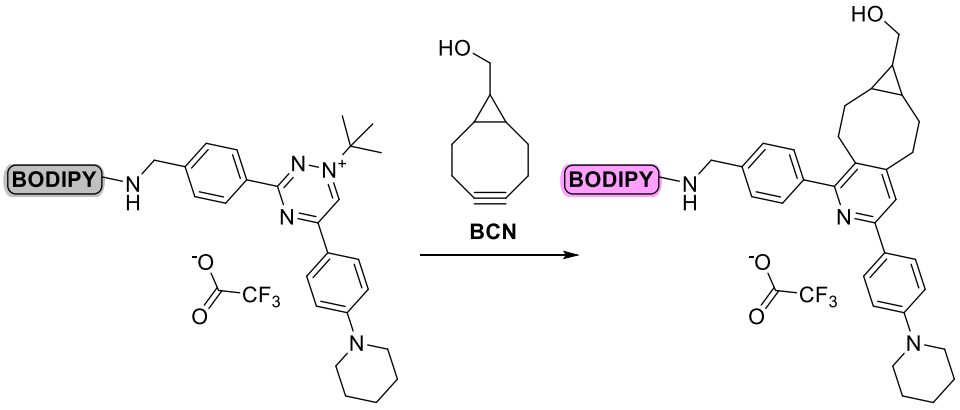

Scheme 19: Fluorescence turn-on of triazinium probes with BCN.

It is apparent from the reaction kinetics, that the fluorescence turn-on is significantly higher in the red-shifted triazinium probes in comparison to the respective tetrazine counterparts (Figure 13).

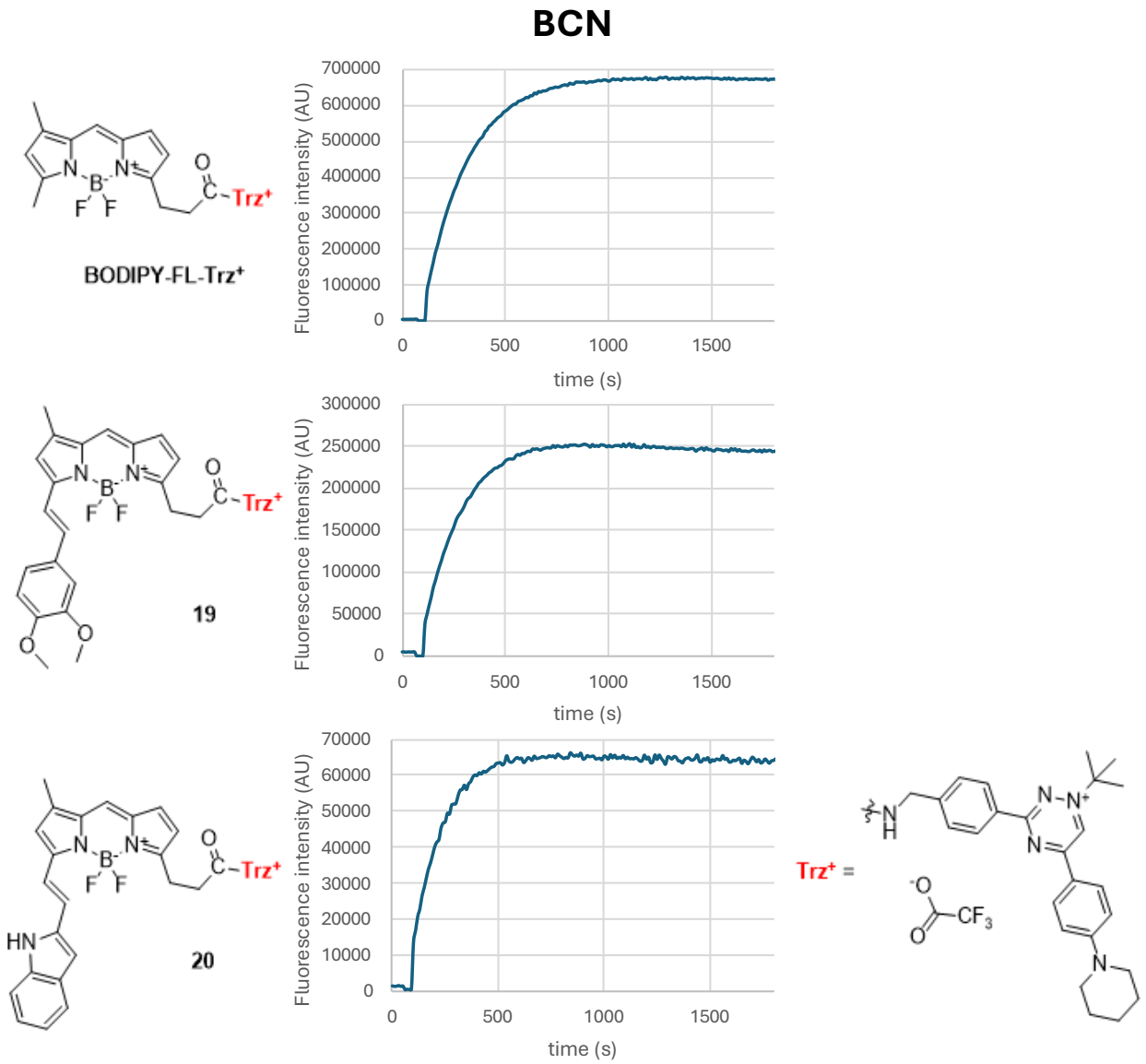

Figure 13: Reaction kinetics of non-conjugated triazinium probes after addition of 1 µL of 0.5M BCN in DMSO (right). Solvent system: 50% MeCN in H_2O. c = 1 µM, V = 1 mL.

Their turn-on values are considerably larger than their tetrazine counterparts (Table 3), due to the superior fluorescence quenching properties of triaziniums (Figure 14). The highest turn-on values are still observed in the non-red-shifted probe **BODIPY-FL-Trz$^+$**, but this is in correlation with the fact that the red-shifted dyes have lower fluorescence intensity by default, before attachment of the quenching triazinium. Also, triaziniums have lower spectral overlap with the red-shifted probes which lowers quenching ability, too, as discussed in Chapter 4.7.

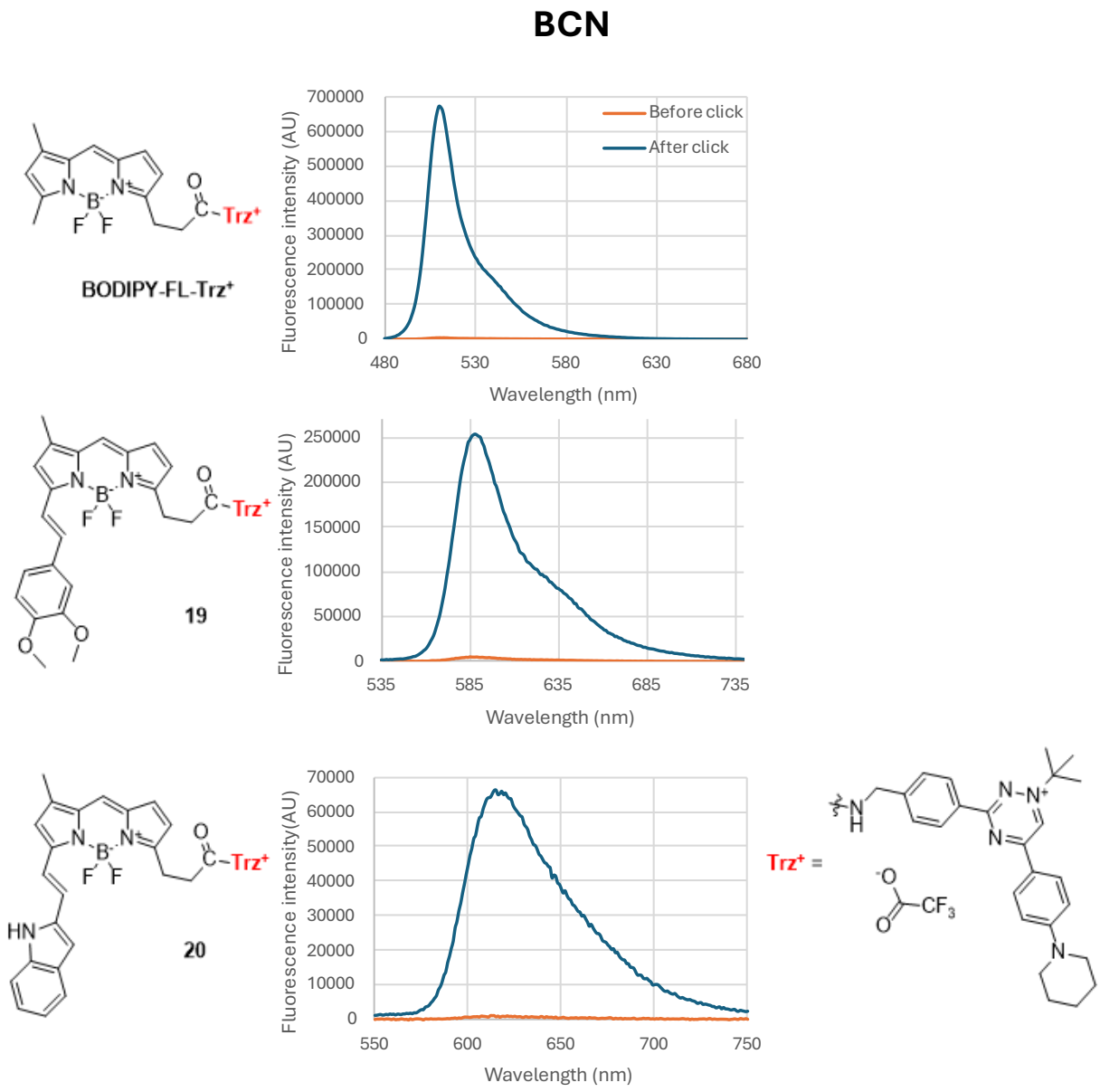

Figure 14: Emission spectra of triazinium probes. Fluorescence was measured before (orange lines) and after (blue lines) the addition of 1 µL of 0.5M BCN in DMSO, approximately 30 min after the addition. Solvent system: 50% MeCN in H_2O. *c* = 1 µM, V = 1 mL.

Table 3: Photophysical properties of the non-conjugated fluorogenic triazinium probes.[a]

Probe	Absorption maxima (nm)	Emission maxima (nm)[b]	Fluorescence turn-on[c]
BODIPY-FL-Trz$^+$	504	510	241
19	573	588	57
20	593	615	93

[a]Solvent system: 50% MeCN in H_2O. c = 1 µM [b]Emission maxima before "click" reaction. [c]Turn-on calculated by dividing the integrated emission areas.

3.6.2 Conjugated tetrazine probe **24**

The photophysical properties of the conjugated BODIPY-tetrazine probe **24** were measured in the same experimental setup as the non-conjugated probes (Chapter 3.6.1). First, absorption maximum of the probe was measured using UV-Vis spectrophotometry. It was found to be at 574 nm, which is an unexpectedly high red-shift comparable to the non-conjugated probes, which were specifically designed and selected to be red-shifted.

Next, spectrofluorometric measurements were conducted both with TCO and BCN as the reaction partners. The expected products of these reactions are shown in Scheme 20.

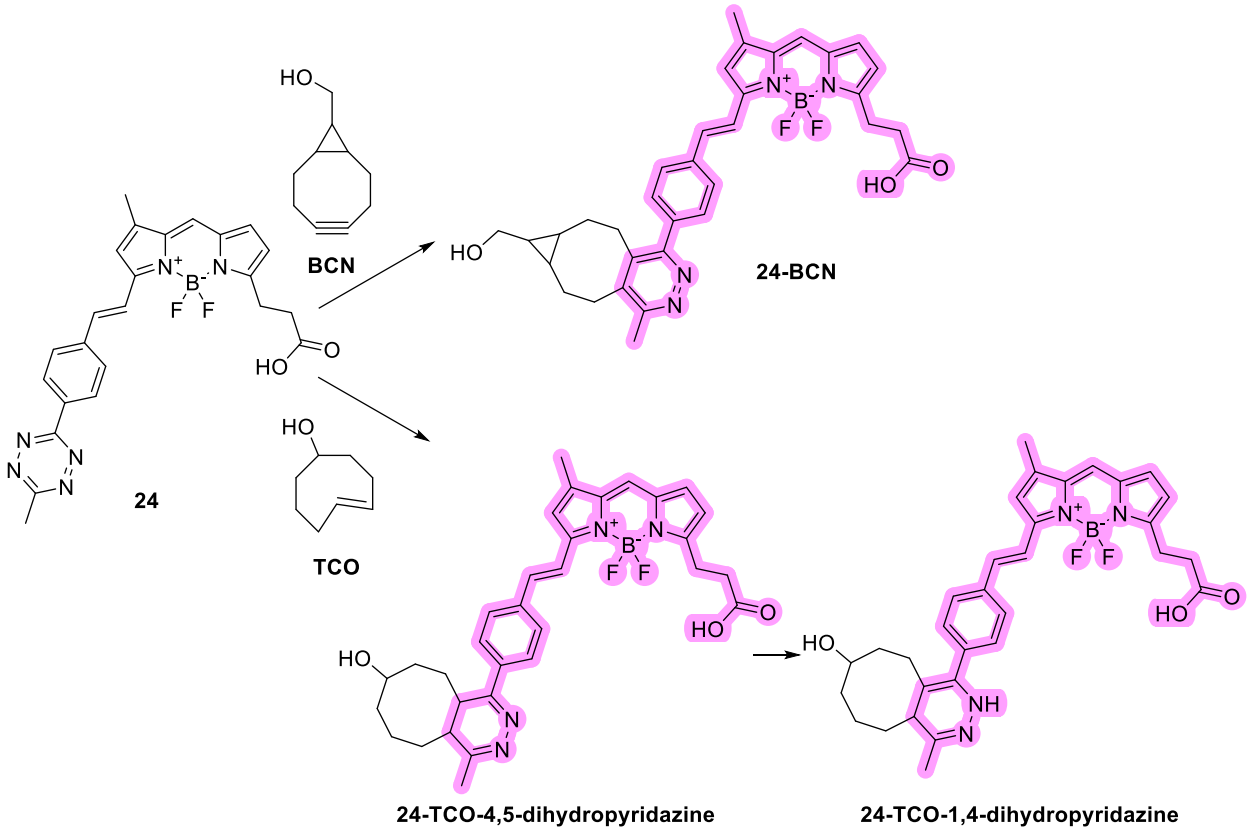

Scheme 20: Fluorescence turn-on of conjugated tetrazine probe with BCN and TCO.

It is apparent from the reaction kinetics measurements that with TCO, the fluorescence intensity reaches a maximum and then drops to significantly lower values where it reaches a plateau (Figure 15 left). This is considered to be due the isomerization to the 1,4-dihydropyridazine product **24-TCO-1,4-dihdropyridazine** that partially quenches the "click" product's fluorescence. On the other hand, with BCN, the fluorescence enhancement is much higher, showing the true strength of fluorescence quenching via a conjugated linker (Figure 15 right).

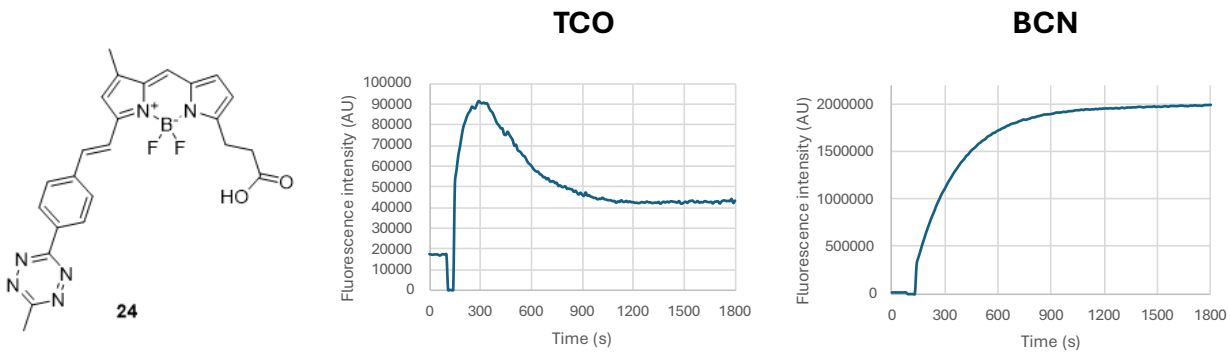

Figure 15: Reaction kinetics of compound **27** after addition of 1 µL of 0.5M TCO in MeOH (left) and 1 µL of 0.5M BCN in DMSO (right). Solvent system: 50% MeCN in H_2O. c = 1 µM, V = 1 mL.

The fluorescence enhancement was calculated by dividing the integrated areas of the whole emission spectra before and after the click. The compared emission spectra before and after the click are represented in Figure 16.

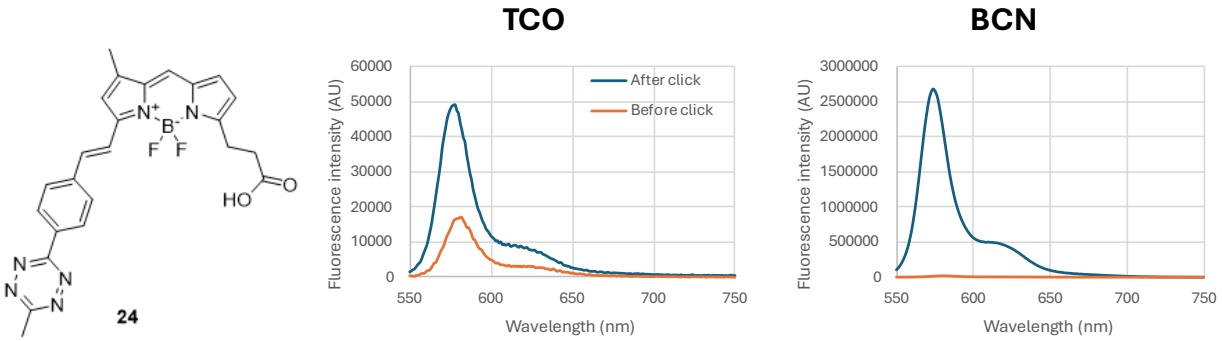

Figure 16: Emission spectra of compound **24** after the reaction with TCO/BCN. Fluorescence was measured before (orange lines) and after (blue lines) the addition of 1 µL of 0.5M TCO in MeOH or 1 µL of 0.5M BCN in DMSO, both approximately 30 min after the addition. Solvent system: 50% MeCN in H_2O. c = 1 µM, V = 1 mL.

It is evident from Figure 16 that TCO is able to turn the fluorescence on to some extent, but it is not comparable with BCN. The fluorescence turn-on values are summarized in Table 4. The turn-on value for the reaction with TCO is 3.0, whereas the corresponding value for BCN reaches a remarkable 149.

Table 4: Photophysical properties of the conjugated fluorogenic tetrazine probe **24**.[a]

Probe	Absorption maximum (nm)	Emission maximum (nm)[b]	Fluorescence turn-on[c]	
			TCO	BCN
24	574	581	3,0	149

[a]Solvent system: 50% MeCN in H_2O. c = 1 µM [b]Emission maxima before "click" reaction. [c]Turn-on calculated by dividing the integrated emission areas.

The great fluorescence turn-on value upon activation by BCN make the compound **24** a very interesting candidate for subsequent experiments. Furthermore, there is a reason to believe that the fluorescence turn-on value could be even higher, because there were still some potentially fluorescent impurities observed on LCMS, which could cause a higher background signal. I was unable to purify the compound any further in fear of losing the little compound that I managed to prepare.

In order to prove the formation of the expected click-product, a series of LCMS experiments was performed to show the mass of the probes after activation (Table 5). Each of the probes were subjected to the "click" reaction with their bioorthogonal counterpart (**TCO**, **BCN**, or both) and after 30 minutes of shaking, the resulting mixture was measured on LCMS.

Table 5: Calculated and found exact masses for products of reactions between the fluorogenic probes and their bioorthogonal counterparts (**TCO** or **BCN**). Exact masses were found using LCMS.[a] ND = not defined.

Probe	Product mass with **TCO** $[M+H]^+$		Product mass with **BCN** $[M+H]^+$	
	Calculated	Found	Calculated	Found
BODIPY-FL-Tz	574.3	574.3	598.3	598.2
16	722.4	722.2	746.4	746.2
17	701.4	701.2	725.4	725.2
BODIPY-FL-Trz+	ND	ND	742.4	742.2
19	ND	ND	890.5	890.2
20	ND	ND	869.5	865.9
24	573.3	573.2	597.3	597.1

[a]The probe was dissolved in acetonitrile (c = 100 µM) and then 1 µL of 0.5M reaction partner (TCO or BCN) was added and the mixture was left to shake for 30 minutes. The resulting solution was analyzed by LCMS.

3.7 Live-cell experiments

To investigate the potential of the synthesized fluorogenic probes for bioimaging applications, a series of live-cell experiments was conducted using the most promising derivatives. After evaluating the results from spectrofluorometric measurements (Chapter 3.6), the non-conjugated tetrazine-based probes **BODIPY-FL-Tz**, **16**, and **17** were all discarded for later experiments due to their insufficient fluorogenic properties. **BODIPY-FL-Tz** by itself showed great fluorescence turn-on values, but it is not red-shifted and its only use for this work would be as a benchmark for the other tetrazine probes. The triazinium probes **BODIPY-FL-Trz$^+$**, **19**, and **20**, on the other hand, all showed great turn-on values and they were selected for live-cell experiments, as well as the probe with conjugated tetrazine **24**. The results from the spectrofluorometric

measurements are summarized in Table 6, explaining the choice of candidates for live-cell imaging.

Table 6: Unified results from spectrofluorometric measurements. Probes selected for live-cell imaging highlighted by green color. ND = not defined

Compound	Fluorescence turn-on	
	TCO	**BCN**
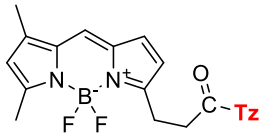 **BODIPY-FL-Tz**	7,9	66
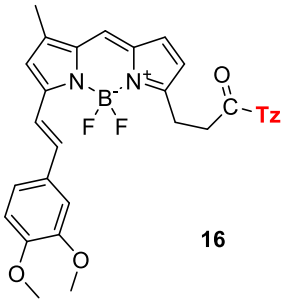 **16**	1,2	4,5
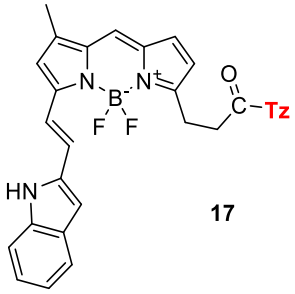 **17**	1,1	2,7
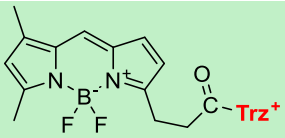 **BODIPY-FL-Trz$^+$**	ND	241

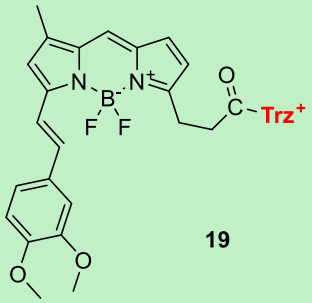 **19**	ND	57
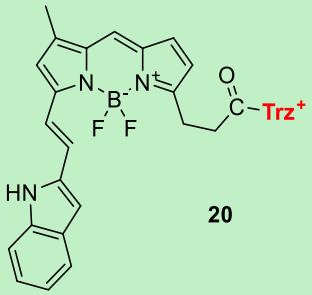 **20**	ND	93
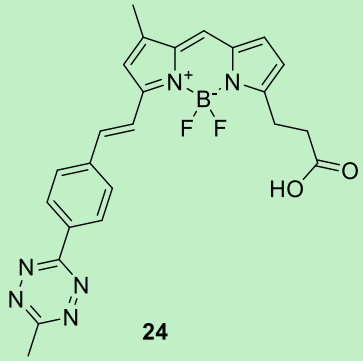 **24**	3,0	149

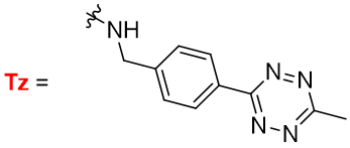

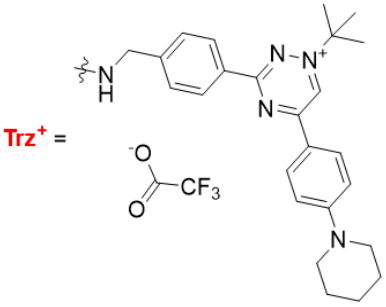

In the first experiment, a reaction of the triazinium-based probes **BODIPY-FL-Trz$^+$**, **19**, and **20** with *endo*-BCN-triphenylphosphonium conjugate (***endo*-BCN-TPP,** Figure 17) was performed in live-cells. ***Endo*-BCN-TPP** is a reagent previously developed in our group.[48]

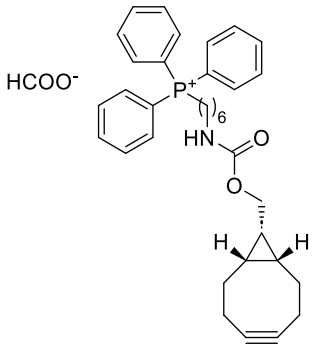

BCN-TPP

Figure 17: Molecular structure of ***endo*-BCN-TPP**

The TPP moiety has high affinity to mitochondria and thus ensures that the bioorthogonal reaction takes place specifically in these subcellular compartments.[49] This experiment by itself does not provide any insight into biochemical processes in living cells, but it is a useful tool for assessing the utility of fluorogenic probes in a biological setting. In confocal microscopy, it is often difficult to draw absolute conclusions from experiments, as the results are primarily qualitative in nature. However, they still provide valuable insights into distribution, behavior, and overall performance of the probe within biological systems.

The experimental setup for mitochondrial visualization was to incubate the cells with ***endo*-BCN-TPP** for 15 min, wash the excess ***endo*-BCN-TPP** and incubate with the fluorogenic probe. Then, the cells were imaged on a confocal microscope without any washing. The controls were obtained by treating the cells only with the fluorogenic probe without ***endo*-BCN-TPP**. The procedure is described in more detail in the Experimental section (Chapter 7). The expected "click" product of the reaction is shown in Scheme 21.

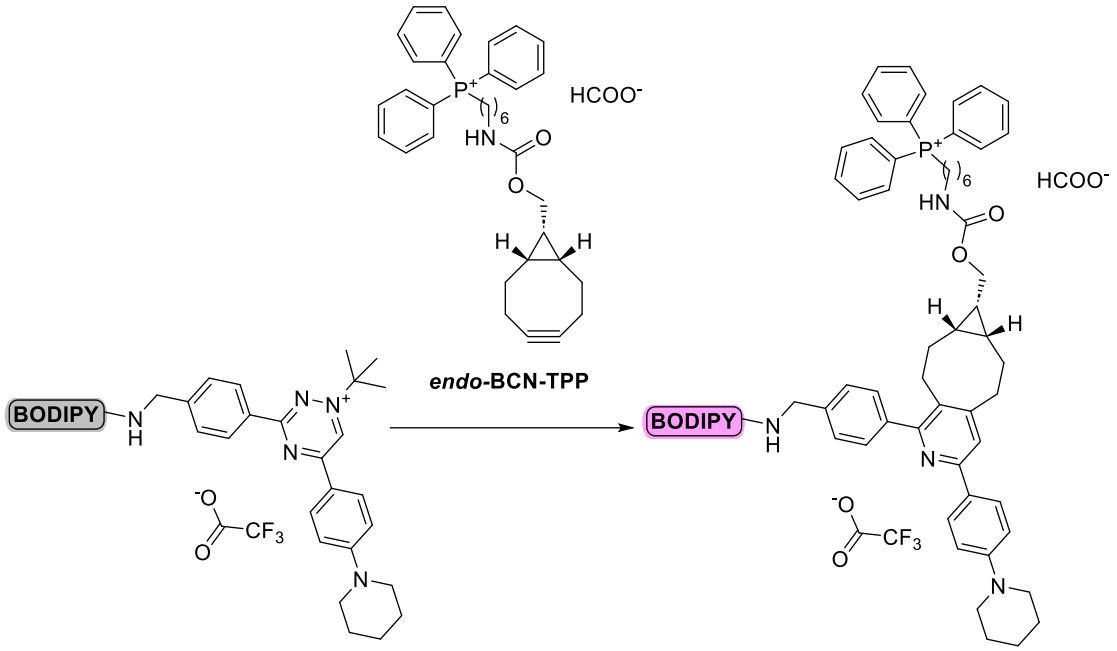

Scheme 21: Live-cell fluorescence turn-on of triazinium probes with ***endo*-BCN-TPP**

All triazinium probes **BODIPY-FL-Trz$^+$**, **19**, and **20** showed the ability to visualize mitochondria in the first series of experiments (Figure 18, cell nuclei stained with green fluorescent nuclear protein and shown in blue). The non-red-shifted probe **BODIPY-FL-Trz$^+$** (Figure 18, **A1**) exhibits brighter fluorescence upon turn-on by ***endo*-BCN-TPP** than its red-shifted counterparts **19** and **20** (Figure 18, **B1** and **C1**, respectively). Out of the two red-shifted probes **19** and **20**, the probe **19** exhibits brighter fluorescence than the probe **20**. Nevertheless, all probes display minimal background fluorescence (Figure 18, bottom row), showcasing their suitability for bioimaging applications.

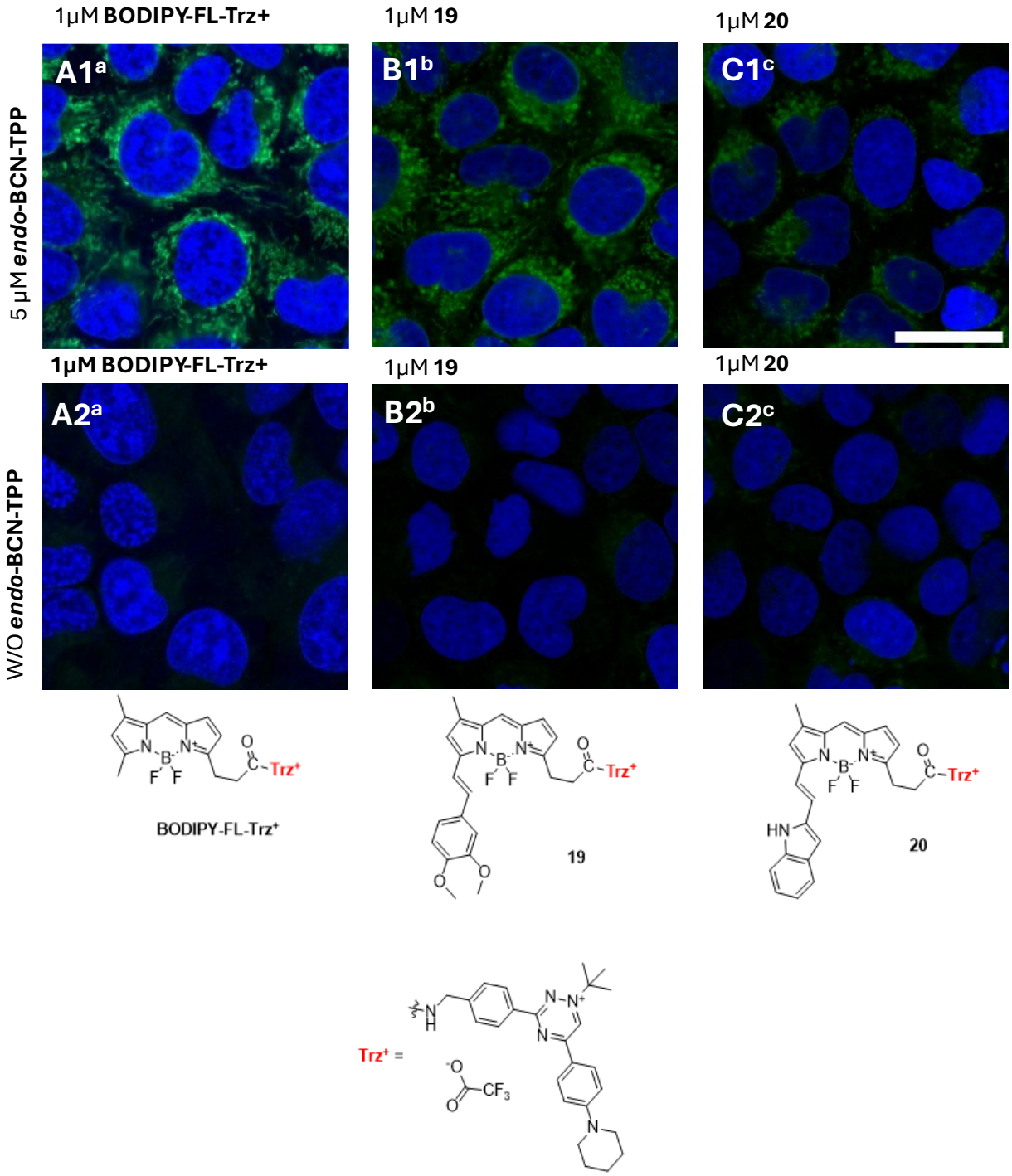

Figure 18: Confocal microscope images of U2OS (H2B SPARK) cells treated with ***endo*-BCN-TPP** conjugate and labeled with A1) **BODIPY-FL-Trz+**, B1) **19**, C1) **20** (3×zoomed). A2) B2) C2) are the corresponding controls (cells treated only with the probe). Click labeling is shown in green. Nuclei were stained with DRAQ5 or visualized by green fluorescent nuclear protein and are shown in blue. [a,b]Microscope set-up: BPTmX-T1 (561 nm) laser intensity: 1.0[a] or 1.5[b] %, and emission (543 – 694 nm) detector: 550[a,b] V. [c]Microscope set-up: BODIPY (488 nm) laser intensity: 2.0 %, and emission (490 – 658 nm) detector: 600 V. DRAQ5 – laser 639 nm. Scale bar is 25 μm.

In the next experiment the probes were used to visualize an *endo*-BCN-dasatinib conjugate (***endo*-BCN-dasatinib**), a BCN-drug conjugate developed by our research group.[42] Dasatinib is a very potent ATP-competitive tyrosine kinase inhibitor which plays an important role in targeted cancer therapy.[50] Its visualization in living cells may shed light on the spatial distribution and other pharmacokinetic and pharmacodynamic properties of this drug.

The experimental setup was the same as in the previous experiment, but ***endo*-BCN-dasatinib** is used instead of ***endo*-BCN-TPP**. Again, the non-red-shifted **BODIPY-FL-Trz$^+$** exhibited brighter fluorescence, but all probes were capable of visualizing the distribution of ***endo*-BCN-dasatinib** in living cells.

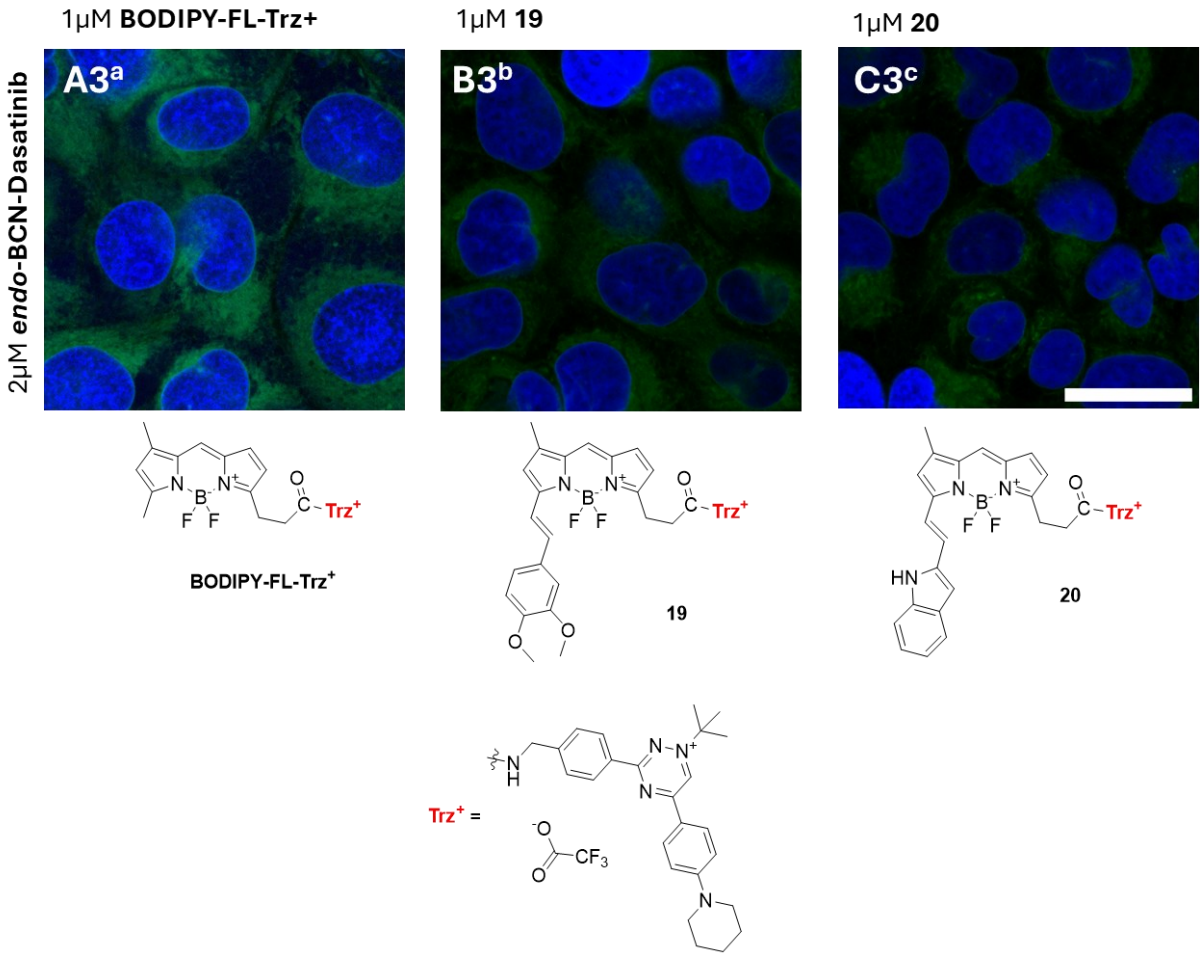

Figure 19: Confocal microscope images of U2OS (H2B SPARK) cells treated with ***endo*-BCN-dasatinib** drug conjugate and labeled with A3) **BODIPY-FL-Trz$^+$**, B3) **19**, C3) **20** (3×zoomed). A2) B2) C2) from **Figure 18** are the corresponding controls (cells treated only with the probe). Click labeling is shown in green. Nuclei were stained with DRAQ5 or visualized by green fluorescent nuclear protein and are shown in blue. [a,b]Microscope set-up: BPTmX-T1 (561 nm) laser intensity: 1.0[a] or 1.5[b] %, and emission (543 – 694 nm) detector: 550[a,b] V. [c]Microscope set-up: BODIPY (488 nm) laser intensity: 2.0 %, and emission (490 – 658 nm) detector: 600 V. DRAQ5 – laser 639 nm. Scale bar is 25 μm.

The results suggest that the fluorogenic triazinium probes **BODIPY-FL-Trz$^+$**, **19**, and **20** are attractive new probes capable of visualizing various targets depending on the experimental setup. Their most prominent features include low background fluorescence in the quenched state and, in the case of probes **19** and **20**, a significant red-shift. This red-shift enhances their suitability for *in vivo* imaging by reducing cytotoxicity and improving tissue penetration of both the excitation and emission light.

The same experiments were repeated with the promising conjugated probe **24**. First, the visualization of mitochondria with ***endo*-BCN-TPP** was performed in the same experimental setup as with the triazinium probes (Figure 20). The higher concentrations (10 μM and 5 μM) were chosen because we expected the probe **24** to have lower cell membrane permeability due to the presence of free carboxylic acid; higher concentration should increase the uptake inside the cells. Also, we could afford to raise the concentration, because the probe has great fluorescence turn-on values and therefore should have very low background noise. At both concentrations, the probe exhibits very low background fluorescence (Figure 20, D3 and D4) and very bright fluorescence upon turn-on by ***endo*-BCN-TPP** (Figure 20, D1 and D2). No observation suggested decreased cell membrane permeability in comparison to the triazinium probes. The fluorescence is evidently concentrated in mitochondria, which proves both the reactivity of the probe **24** towards ***endo*-BCN-TPP** and also the bioorthogonality to endogenous functional groups (low background fluorescence suggests no reaction happens before the introduction of ***endo*-BCN-TPP**).

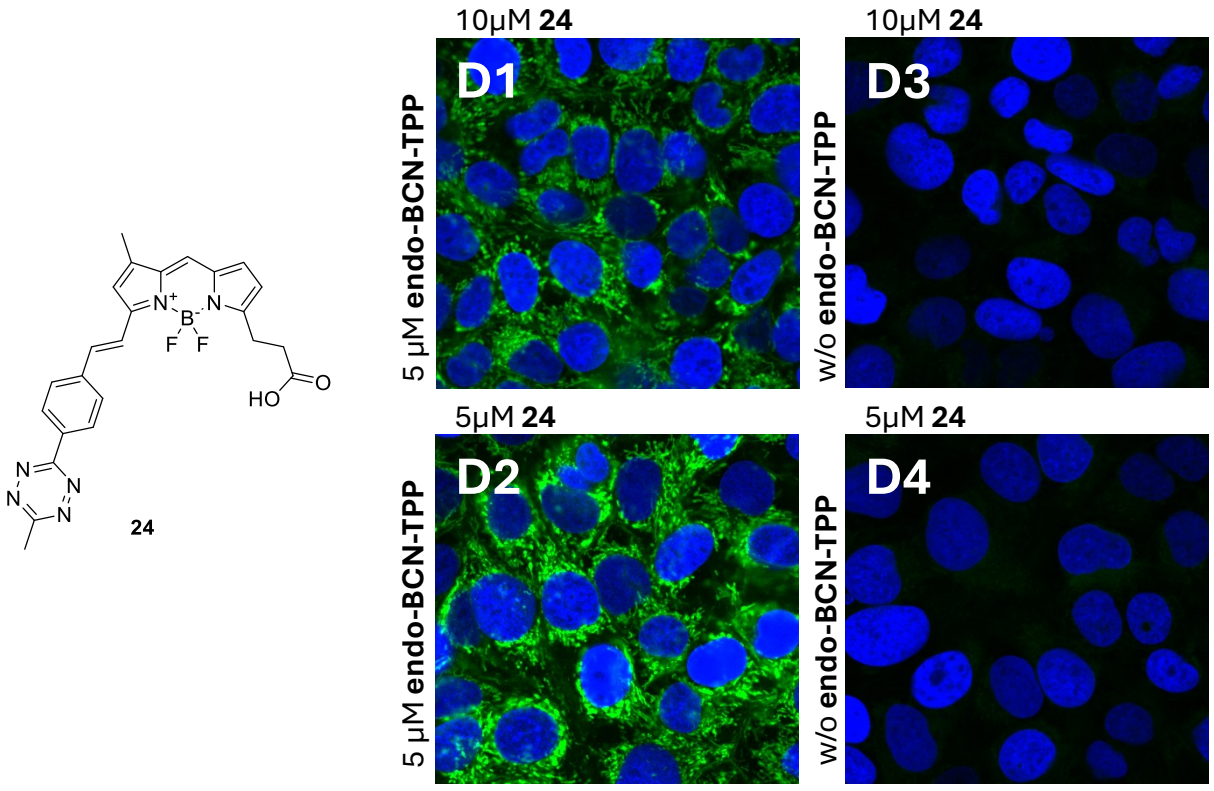

Figure 20: Confocal microscope images of U2OS (H2B SPARK) cells treated with ***endo*-BCN-TPP** conjugate and labeled with D1) 10 µM **24** and D2) 5 µM **24**. D3) and D4) are the corresponding controls (cells treated only with the probe). Click labeling is shown in green. Nuclei were stained with DRAQ5 or visualized by green fluorescent nuclear protein and are shown in blue. [a,b]Microscope set-up: BPTmX-T1 (561 nm) laser intensity: 1.0[a] or 1.5[b] %, and emission (543 – 694 nm) detector: 550[a,b] V. [c]Microscope set-up: BODIPY (488 nm) laser intensity: 2.0 %, and emission (490 – 658 nm) detector: 600 V. DRAQ5 – laser 639 nm.

Then, the small molecule visualization of ***endo*-BCN-dasatinib** was performed with the probe **24** in the same experimental setup as with the triazinium probes. Again, the probe showed very low background fluorescence (Figure 21, D7 and D8) and great fluorescence turn-on upon activation by ***endo*-BCN-dasatinib** (Figure 21, D5 and D6).

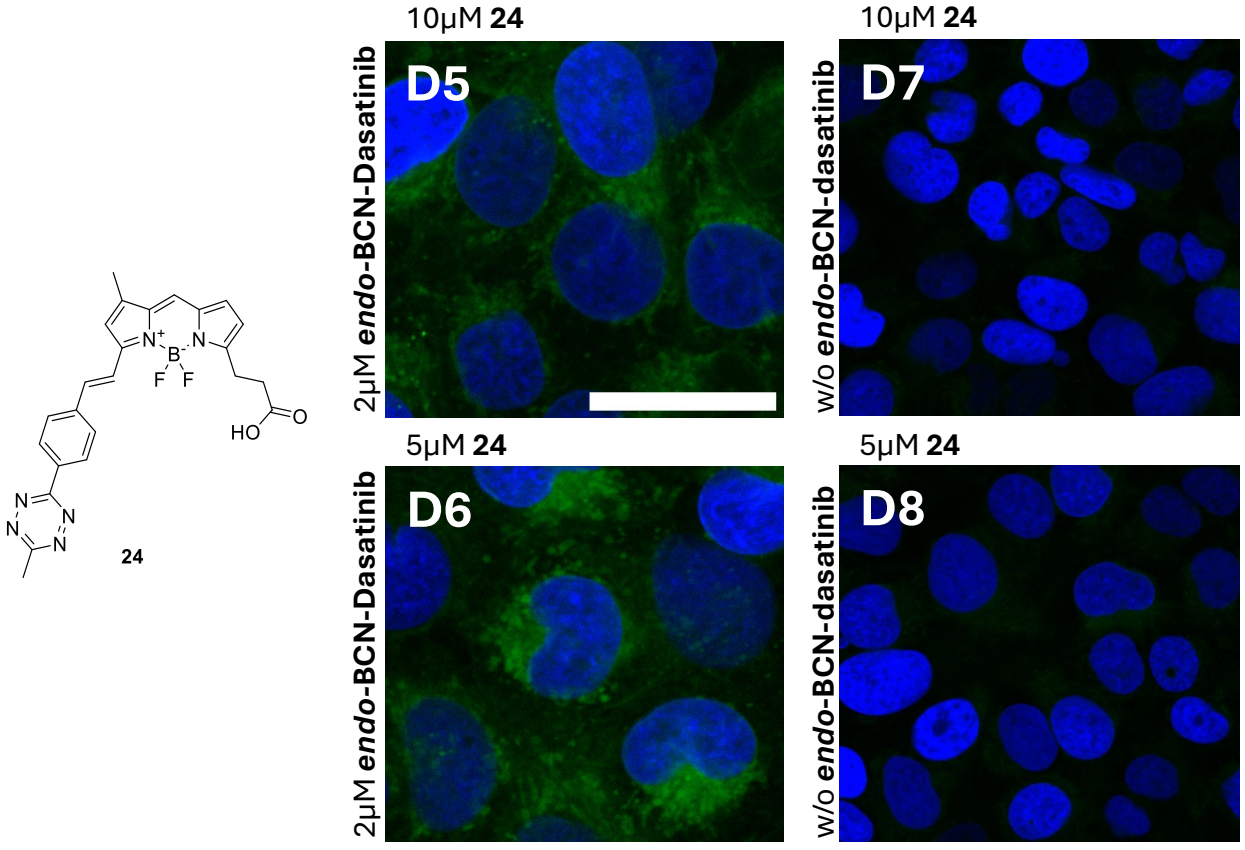

Figure 21: Confocal microscope images of U2OS (H2B SPARK) cells treated with ***endo*-BCN-dasatinib** drug conjugate and labeled with A3) **BODIPY-FL-Trz$^+$**, B3) **19**, C3) **20** (3×zoomed). A2) B2) C2) from **Figure 18** are the corresponding controls (cells treated only with the probe). Click labeling is shown in green. Nuclei were stained with DRAQ5 or visualized by green fluorescent nuclear protein and are shown in blue. [a,b]Microscope set-up: BPTmX-T1 (561 nm) laser intensity: 1.0[a] or 1.5[b] %, and emission (543 – 694 nm) detector: 550[a,b] V. [c]Microscope set-up: BODIPY (488 nm) laser intensity: 2.0 %, and emission (490 – 658 nm) detector: 600 V. DRAQ5 – laser 639 nm. Scale bar is 25 μm.

The two experiments, one with ***endo*-BCN-TPP** and the other with ***endo*-BCN-dasatinib**, prove that the conjugated probe **24** possesses great fluorogenic properties even in live-cell experiments. After synthesis, we were concerned that low solubility or potential instability might compromise the experiments, however, none of the issues manifested during testing. The conjugated probe **24** proved to be far superior to all red-shifted probes containing a fluorescence-quenching moiety linked via a non-conjugated spacer, particularly in terms of fluorescence turn-on efficiency.

3.7 Conclusion

In this work, I focused on the design, synthesis and testing of novel bioorthogonally active red-shifted fluorogenic probes for bioimaging applications.

First of all, **BODIPY-FL** was prepared in large scale based on previously published procedure.[43]

Then, red-shifted **BODIPY-FL** derivatives were prepared by extending the conjugation of the green-emitting dye. **BODIPY-FL** derivatives showing both good synthetic availability and red-shift were identified in a series of small-scale reactions analyzed by LCMS. The most attractive candidates were then further derivatized by installation of a tetrazine or triazinium as a fluorescence quenching group *via* a non-conjugated flexible linker.

To demonstrate the difference in fluorescence quenching properties between quenchers linked through a non-conjugated flexible linker and those linked *via* a conjugated system, a **BODIPY-FL** derivative bearing a directly conjugated tetrazine was prepared.

The fluorogenic properties of all compounds were then investigated using spectrofluorometric measurements. The non-conjugated tetrazine derivatives **BODIPY-FL-Tz**, **16**, and **17** did not show great results in terms of fluorescence turn-on upon reaction with their bioorthogonal counterparts (**BCN** and **TCO**). On the other hand, the non-conjugated triazinium probes **BODIPY-FL-Trz$^+$**, **19**, and **20** showed great fluorescence turn-on values upon reaction with **BCN** and they were proved to exhibit fluorogenic properties in live-cell experiments as well.

A fluorogenic probe **24** bearing a directly conjugated tetrazine was prepared as well and it showed great results in terms of fluorescence turn-on values and proved to be very efficient even in live-cell experiments. This probe was far superior even to the promising triazinium-containing probes, showcasing the strength of fluorescence quenching *via* conjugated spacers. Consequently, we believe that an analogous derivative having a conjugated triazinium instead of a tetrazine could be even more efficient in terms of fluorescence quenching efficiency. However, this compound was not synthesized due to time constraints, and thus represents an attractive direction for future research.

4. Experimental section

4.1 General methods

Solvents and other commercially available chemicals were purchased from common suppliers (Sigma-Aldrich, Fluorochem, abcr, Lach-Ner, Penta). Dry solvents were purchased from Acros Organics B.V.B.A with molecular sieves.

Reactions were monitored with TLC silica gel 60 F254 purchased from Merck. They were analyzed with a UV lamp at wavelengths 254 nm or 365 nm. Reactions were also monitored with HPLC-MS (Shimadzu LCMS-2020) in gradient of water/acetonitrile with 0.05% formic acid at the column CORTECS C18+ Column, 90 Å, 2.7 µm, 4.6 mm X 50 mm, 1/pk.

Isolation of products was performed using silica gel 40-60 µm. For reversed-phase chromatography RediSep Rf Gold® C18 columns were used. Combiflash Rf+ was used for flash column chromatography.

1H and 13C spectra were measured on Bruker Avance IIITM HD 400 MHz Prodigy or Bruker Avance IIITM HD 400 MHz. NMR assignments were done based on 1D (1H, APT) and 2D (COSY, HSQC, HMBC) NMR experiments. NMR spectra of compound **24** were measured on Bruker Avance III™ HD 600 MHz. Chemical shifts were referenced to the used solvent. High-resolution mass spectra were recorded on Agilent 5975C MSD Quadrupol or LTQ Orbitrap XL from Thermo Fisher Scientific.

Evaporation of volatiles was performed with VACUUBRAND™ PC3001 VARIO™ Pro Pumping System. Lyophilization was performed using either BUCHI LyovaporTM L-300 Freeze Dryer or FreeZone Plus 2.5 Liter Cascade Benchtop Freeze Dry System.

Fluorescence measurements were performed on a FluoMax4 spectrofluorometer (Jobin Yvon, Horiba).

Cellular imaging experiments were performed by ZEISS LSM 980 confocal microscope (40×W objective).

4.2 Synthesis

Benzyl 2-(dimethoxyphosphoryl)acetate (**2**)

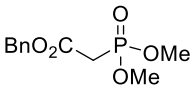

Compound **2** was synthesized according to a previously reported methodology.[51] A neat mixture of benzyl bromoacetate **7** (5.00 g, 21.83 mmol) and trimethyl phosphite **8** (6.12 g, 49.33 mmol) was stirred vigorously for 20 h under condenser (MeBr evolution). The reaction was monitored by TLC (PE/AcOEt 1/1, stained by $KMNO_4$) and by LCMS. The volatiles were evaporated under reduced pressure and the product was purified using flash column chromatography (0-100 % AcOEt in PE) to give **2** as a colorless oil (4.00 g, 71 % yield). **^{1}H NMR (401 MHz, DMSO)**: δ (ppm) = 7.43 – 7.28 (m, 5H), 5.15 (s, 2H), 3.65 (d, *J* = 11.2 Hz, 6H), 3.26 (d, *J* = 21.4 Hz, 2H). Spectra are in accordance with literature.[51]

Benzyl (2E)-3-(1H-pyrrol-2-yl)prop-2-enoate (**3**)

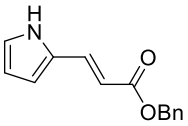

Compound **3** was prepared according to a previously published procedure.[43] To a solution of benzyl 2-(dimethoxyphosphoryl)acetate (**2**) (4.00 g, 15.49 mmol) in dry THF (20 mL) was added NaH (682 mg, 17.04 mmol, 60 % in mineral oil) in several portions at 0 °C. The resulting solution was left to stir for 10 min. After the reaction mixture turned white (due to deprotonation of **2**), a solution of 1H-pyrrole-2-carbaldehyde **1** (1.62 g, 17.04 mmol) in dry THF (8 mL) was added dropwise to the reaction mixture at 0 °C over the course of 5 min. The reaction mixture was left to stir at r.t. for 1.5 h. The reaction was monitored by LCMS. The reaction was quenched with 5% citric acid aqueous solution, diluted with water and extracted with 3x50 mL of EtOAc. The combined organic layers were washed with water, brine, dried over $MgSO_4$ and concentrated *in vacuo*. Then, the mixture was dry loaded on silicagel column and it was eluted in PE/AcOEt 4/1 to give **3** as a white solid (1.60 g, 45 % yield). **^{1}H NMR (401 MHz, DMSO)**: δ (ppm) = 11.53 (s, 1H), 7.49 (d, *J* = 15.8 Hz, 1H), 7.41 – 7.29 (m, 5H), 7.03 (td, *J* = 2.7, 1.4 Hz, 1H), 6.59 (p, *J* = 1.6 Hz, 1H), 6.25 (d, *J* = 15.8 Hz, 1H), 6.16 (dt, *J* = 3.5, 2.3 Hz, 1H), 5.17 (s, 2H). Spectra are in accordance with literature.[43]

Benzyl 3-(1*H*-pyrrol-2-yl)propanoate (**4**)

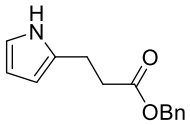

Compound **4** was prepared according to a previously published procedure.[43] Compound **3** (1.27 g, 5.59 mmol) was dissolved in dry methanol. Then Ph_2S (4.68 µL, 27.94 µmol) and Pd/C (178 mg, 167.65 µmol, 10 wt. %) were added under Ar atmosphere. The reaction mixture was equipped with a H_2 balloon and was stirred at r.t. for 7 h. The mixture was filtered over celite, washed with MeOH and concentrated *in vacuo*. The product was purified using silicagel column chromatography (PE/AcOEt 16/1-4/1) to give **4** as a colorless oil (1.23 g, 96 % yield). **^{1}H NMR (401 MHz, DMSO)**: δ (ppm) = 10.53 (s, 1H), 7.72 – 7.04 (m, 5H), 6.57 (m, 1H), 5.86 (m, 1H), 5.73 (m, 1H), 5.09 (s, 2H), 2.81 (m, 2H), 2.73 – 2.62 (m, 2H). Spectra are in accordance with literature.[43]

3-{2-[(3,5-Dimethyl-1H-pyrrol-2-yl-κ*N*)methylidene]-2H-pyrrol-5-yl κ*N*}propanoatato)(difluoro)boron (**6**)

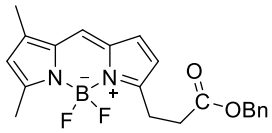

Compound **6** was prepared according to a previously published procedure.[43] To a solution of **4** (1.01g, 4.41 mmol) and 3,5-dimethyl-1*H*-pyrrole-2-carbaldehyde **5** in dry $PhCF_3$ (25 mL) was added $POCl_3$ (452 µL, 4.85 mmol) dropwise at 0 °C under argon atmosphere. The reaction mixture was stirred at r.t. for 2 h and then cooled to 0 °C. Then, $BF_3{\cdot}Et_2O$ (2.17 mL, 17.64 mmol) was added to the mixture followed by addition of DIPEA over the course of 5 min. The reaction mixture was left to gradually reach r.t. After 2.5 h, the reaction mixture was cooled to 0 °C and diluted with 5% $NaHCO_3$ aqueous solution. The reaction mixture was then extracted with 3x50 mL of AcOEt. The combined organic layers were washed with water, brine, dried over $MgSO_4$ and concentrated *in vacuo*. The product was purified using silicagel column chromatography (PE/AcOEt 4/1) to give **6** as a reddish green solid (1.15 g, 68% yield). **^{1}H NMR (401 MHz, DMSO):** δ (ppm) = 7.71 (s, 1H), 7.51 – 7.16 (m, 5H), 7.07 (d, *J* = 4.0 Hz, 1H), 6.36 (d, *J* = 4.0 Hz, 1H), 6.31 (s, 1H), 5.13 (s, 2H), 3.14 (t, 2H), 2.90 – 2.73 (t, 2H), 2.47 (s, 3H), 2.26 (s, 3H). Spectra are in accordance with literature.[43]

BODIPY FL propionic acid (**BODIPY-FL**)

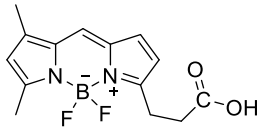

BODIPY-FL was prepared according to previously published procedure.[43] Compound **6** (1.15 g, 3.00 mmol) and Pd/C (63.76 mg, 59.91 µmol, 10 wt. %) were dissolved in dry MeOH (20 mL) under argon atmosphere. The

reaction vessel was equipped with H_2 balloon and it was stirred at r.t. for 2 h. The catalyst was removed by filtration over celite, washed with MeOH and AcOEt and the filtrate was concentrated *in vacuo* to give **BODIPY-FL** (850 mg, 97 % yield) as a reddish green solid which was used without further purification. **^{1}H NMR (401 MHz, DMSO)**: δ (ppm) = 12.28 (s, 1H), 7.70 (s, 1H), 7.09 (d, J = 4.0 Hz, 1H), 6.38 (d, J = 4.0 Hz, 1H), 6.31 (s, 1H), 3.07 (m, 2H), 2.73 – 2.60 (m, 2H), 2.48 (s, 3H), 2.26 (s, 3H). Spectra are in accordance with literature.[43]

(3-(7-(3,4-Dimethoxystyryl)-5,5-difluoro-9-methyl-5H-4λ^4,5λ^4-dipyrrolo[1,2-c:2',1'-f][1,3,2]diazaborinin-3-yl)propanoic acid (**10**)

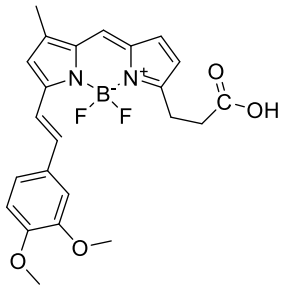

BODIPY FL (100 mg, 342.36 µmol) and 3,4-dimethoxybenzaldehyde **9** (341.35 mg, 2.05 mmol) were dissolved in dry MeCN (10 mL) under argon atmosphere. Then, pyrrolidine (286 µL, 3.42 mmol) and AcOH(196 µL, 3.42 mmol) were added dropwise and the reaction mixture was stirred for 2.5 h at r.t. The reaction was monitored by LCMS. Longer reaction times (3+ hours) cause decomposition of the product. The crude reaction mixture was concentrated *in vacuo* and the product was purified by silicagel column chromatography eluted with AcOEt followed by RP flash column chromatography for further purification to give compound (80 mg, 53 % yield) as a reddish blue solid. **^{1}H NMR (401 MHz, DMSO)**: δ (ppm) = 12.31zyz (s, 1H), 7.63 (m, 2H), 7.27 (m, 2H), 7.16 (d, *J* = 2.0 Hz, 1H), 7.09 – 7.01 (m, 3H), 6.39 (d, *J* = 3.9 Hz, 1H), 3.83 (d, *J* = 6.8 Hz, 6H), 3.12 (t, 2H), 2.67 (t, 2H), 2.31 (s, 3H). **^{13}C NMR (101 MHz, DMSO)**: δ (ppm) = 174.00, 157.14, 156.39, 151.15, 149.49, 143.95, 140.25, 136.64, 133.76, 129.09, 128.14, 123.61, 121.74, 117.47, 116.69, 115.88, 112.56, 110.90, 56.05 (d), 32.72, 24.07, 11.56. **HRMS (ESI):** calcd. for $C_{23}H_{22}BF_2N_2O_4$ $[M-H]^-$ 439.16462, found 439.16438.

3-(7-(2-(1H-indol-2-yl)vinyl)-5,5-difluoro-9-methyl-5H-4λ^4,5λ^4-dipyrrolo[1,2-c:2',1'f][1,3,2]diazaborinin-3-yl)propanoic acid (**12**)

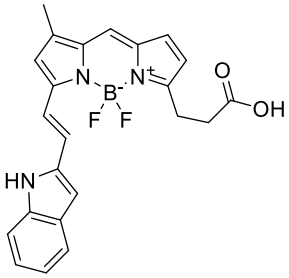

BODIPY FL (50 mg, 171.18 µmol) and 1H-indole-2-carbaldehyde **11** (149 mg, 1.03 mmol) were dissolved in dry MeCN (5 mL) under argon atmosphere. Then, pyrrolidine (143 µL, 1.71 mmol) and AcOH (98 µL, 1.71 mmol) were added dropwise and the reaction mixture was stirred for 2 h at r.t. The reaction was monitored by LCMS. Longer reaction times (3+ hours) cause decomposition of the product. The crude reaction mixture was concentrated *in vacuo* and the product was purified by silicagel column chromatography eluted with AcOEt followed by RP flash column chromatography for further purification to give **12** (34 mg, 47 % yield) as a reddish blue solid. **^{1}H NMR (401 MHz, DMSO)**: δ (ppm) = 11.78 (m, 1H), 7.73 – 7.53 (m, 3H), 7.46 – 7.35 (m, 2H), 7.25 – 7.15 (m, 1H), 7.12 – 6.97 (m, 3H), 6.82 (d, J = 2.0 Hz, 1H), 6.40 (d, J = 4.0 Hz, 1H), 3.21 – 3.05 (m, 2H), 2.68 (dd, J = 9.2, 6.5 Hz, 2H), 2.32 (s, 3H). **^{13}C NMR (101 MHz, DMSO):** δ (ppm) = 173.53, 156.54, 155.69, 143.35, 138.84, 136.46, 135.66, 133.35, 129.97, 128.15, 127.48, 123.88, 122.80, 120.91, 119.82, 117.25, 116.33, 115.74, 111.63, 108.27, 32.47, 23.70, 11.09. **HRMS (ESI):** calcd. for $C_{23}H_{20}BF_2N_3O_2$ $[M+H]^+$ 420.16894, found 420.16864.

tert-Butyl (4-(6-methyl-1,2,4,5-tetrazin-3-yl)benzyl)carbamate (**14**)

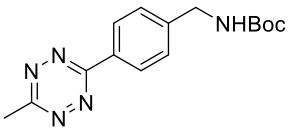

tert-Butyl (4-cyanobenzyl)carbamate **13** (1.00 g, 4.31 mmol) and $Zn(OTf)_2$ (782 mg, 2.15 mmol) were dissolved in dry MeCN (5.22 mL, 43.05 mmol). Then, hydrazine monohydrate (5.22 mL, 107.63 mmol) was added and the reaction mixture was left to stir at 60 °C for 14 h under argon atmosphere. The reaction was monitored using LCMS and TLC (PE/AcOEt 3/2). Then, the reaction mixture was transferred to an Erlenmeyer flask, $NaNO_2$ (5.94 g, 86.10 mmol) was added followed by slow addition of 2M HCl aqueous solution until pH ~ 3. (This step generates **highly toxic** nitrogen oxide gases and should be performed in a well ventilated fume hood).[52] The reaction mixture was left to stir at r.t. for 1 h. The mixture was extracted with 3x40 mL of DCM and the combined organic layers were washed with water, brine, dried over $MgSO_4$ and concentrated *in vacuo*. The product was purified using silicagel column chromatography (0-40 % AcOEt in PE) to give **14** (396 mg, 31 % yield) as a purple solid. **^{1}H NMR (401 MHz, $CDCl_3$)**: δ (ppm) = 8.72 – 8.30 (m, 2H), 7.50 (d, *J* = 8.3 Hz, 2H), 4.43 (d, *J* = 6.2 Hz, 2H), 3.09 (s, 3H), 1.48 (s, 9H). Spectra are in accordance with literature.[45]

(4-(6-methyl-1,2,4,5-tetrazin-3-yl)phenyl)methanamine (**15**)

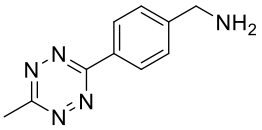

Compound **14** was dissolved in dry DCM (4 mL) and 4M HCl solution in dioxane (4mL) was added dropwise. The reaction mixture was left to stir for 1 h under argon atmosphere. The reaction mixture was concentrated *in vacuo* to give **15** (240 mg, 99 % yield) as a pink solid. **^{1}H NMR (401 MHz, CDCl3)**: δ (ppm) = 8.68 – 8.43 (m, 2H), 7.71 – 7.36 (m, 2H), 4.02 (s, 2H), 3.11 (s, 3H). Spectra are in accordance with literature.[45]

5-Fluoro-7,9-dimethyl-3-(3-((4-(6-methyl-1,2,4,5-tetrazin-3-yl)benzyl)amino)-3-oxopropyl)-5H-dipyrrolo[1,2-c:2',1'-f][1,3,2]diazaborinin-4-ium fluoride (**BODIPY-FL-Tz**)

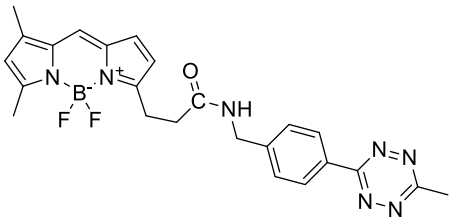

BODIPY-FL (20 mg, 68.47 µmol), Pyoxim (90 mg, 171.2 µmol) and oxyma (24 mg, 171.2 µmol) were dissolved in dry DMF (3 mL) and the mixture was left to stir for 10 min at r.t. The reaction mixture was cooled to 0 °C and the tetrazine **15** (20.67 mg, 102.71 µmol) was added along with DIPEA (36 µL, 205.41 µmol). The mixture was left to stir at r.t. for 2.5 h. The reaction was monitored using TLC (50 % AcOEt in PE) and LCMS. Then, volatiles were evaporated *in vacuo* and the product was purified using silicagel column chromatography (25-100% AcOEt in PE) to give **BODIPY-FL-Tz** (20 mg, 61 % yield) as an orange-red solid. **^{1}H NMR (401 MHz, CDCl3)**: δ (ppm) = 8.64 – 8.23 (m, 2H), 7.44 – 7.29 (m, 2H), 7.10 (s, 1H), 6.89 (d, J = 4.0 Hz, 1H), 6.31 (d, J = 4.0 Hz, 1H), 6.08 (s, 1H), 4.50 (d, J = 5.9 Hz, 2H), 3.32 (t, J = 7.3 Hz, 2H), 3.09 (s, 3H), 2.77 (t, J = 7.3 Hz, 2H), 2.53 (s, 3H), 2.23 (s, 3H). Spectra are in accordance with literature.[53]

3-(7-(3,4-Dimethoxystyryl)-5,5-difluoro-9-methyl-5H-4λ^4,5λ^4-dipyrrolo[1,2-c:2',1'-f][1,3,2]diazaborinin-3-yl)-N-(4-(6-methyl-1,2,4,5-tetrazin-3-yl)benzyl)propanamide (**16**)

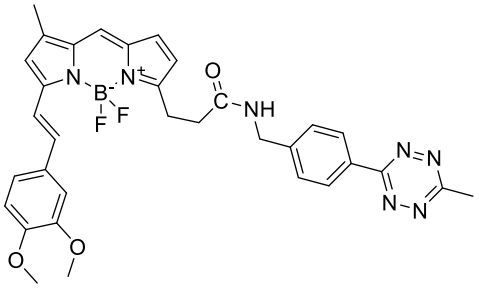

Compound **10** (21 mg, 47.70 µmol), Pyoxim (63 mg, 119.3 µmol) and oxyma (17 mg, 119.3 µmol) were dissolved in dry DMF (3 mL) and the mixture was left to stir for 10 min at r.t. The reaction mixture was cooled to 0 °C and the tetrazine **15** (14.4 mg, 71.55 µmol) was added along with DIPEA (25 µL, 143.1 µmol). The mixture was left to stir at r.t. for 2.5 h. The reaction was monitored using TLC (50 % AcOEt in PE) and LCMS. Then, volatiles were evaporated *in vacuo* and the product was purified using silicagel column chromatography (25-100% AcOEt in PE) to give compound **16** (21 mg, 71 % yield) as a reddish blue solid. **^{1}H NMR (401 MHz, DMSO)**: δ (ppm) = 8.61 (t, J = 6.0 Hz, 1H), 8.42 (d, J = 8.4 Hz, 2H), 7.71 – 7.60 (m, 2H), 7.53 (d, J = 8.3 Hz, 2H), 7.34 – 7.20 (m, 2H), 7.15 (d, J = 2.0 Hz, 1H), 7.10 – 7.01 (m, 3H), 6.39 (d, J = 4.0 Hz, 1H), 4.43 (d, J = 5.9 Hz, 2H), 3.82 (d, J = 4.1 Hz, 6H), 3.19 (t, J = 7.7 Hz, 2H), 2.99 (s, 3H), 2.65 (t, J = 7.7 Hz, 2H), 2.31 (s, 3H). **^{13}C NMR (101 MHz, DMSO):** δ (ppm) = 171.17, 167.09, 163.19, 156.58 (d, J = 17.3 Hz), 150.66, 149.02, 144.37, 143.37, 139.63, 136.10, 133.32, 130.40, 128.64, 128.12, 127.78, 127.41, 123.12, 121.25, 116.93, 116.40, 115.46, 112.09, 110.38, 55.64, 55.55, 41.96, 38.82, 33.74, 24.11, 20.83, 11.11. **HRMS (ESI):** calcd. for $C_{33}H_{31}BF_2N_7O_3$ $[M-H]^-$ 622.25550, found 622.25550.

3-(7-(2-(1H-indol-2-yl)vinyl)-5,5-difluoro-9-methyl-5H-4λ^4,5λ^4-dipyrrolo[1,2-c:2',1'-f][1,3,2]diazaborinin-3-yl)-N-(4-(6-methyl-1,2,4,5-tetrazin-3-yl)benzyl)propenamide (**17**)

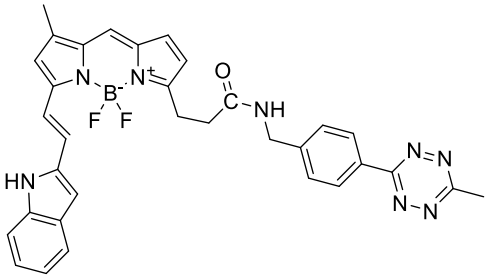

Compound **12** (24 mg, 27.25 µmol), Pyoxim (75 mg, 143.1 µmol) and oxyma (20 mg, 143.1 µmol) were dissolved in in dry DMF (3 mL) and the mixture was left to stir for 10 min at r.t. The reaction mixture was cooled to 0 °C and the tetrazine **15** (17.28 mg, 85.87 µmol) was added along with DIPEA (30 µL, 171.8 µmol). The mixture was left to stir at r.t. for 2.5 h. The reaction was monitored using TLC (50 % AcOEt in PE) and LCMS. Then, volatiles were evaporated *in vacuo* and the product was purified using silicagel column chromatography (25-80% AcOEt in PE) to give compound **17** (15 mg, 43 % yield) as a blue solid. **^{1}H NMR (401 MHz, DMSO)**: δ (ppm) = 11.76 (d, J = 2.2 Hz, 1H), 8.61 (t, J = 5.9 Hz, 1H), 8.49 – 8.11 (m, 2H), 7.72 – 7.60 (m, 2H), 7.55 (m, 3H), 7.44

– 7.35 (m, 2H), 7.17 (m, 1H), 7.11 – 6.96 (m, 3H), 6.81 (d, J = 2.0 Hz, 1H), 6.39 (d, J = 4.0 Hz, 1H), 4.44 (d, J = 5.9 Hz, 2H), 3.21 (t, J = 7.8 Hz, 2H), 2.99 (s, 3H), 2.72 – 2.62 (m, 2H), 2.32 (d, J = 3.1 Hz, 3H). **^{13}C NMR (101 MHz, DMSO)**: δ (ppm) = 171.60, 167.53, 163.66, 156.88, 144.82, 143.61, 139.27, 136.83, 136.11, 133.79, 130.86, 130.25, 128.61, 127.95, 127.88, 124.27, 123.16, 121.30, 120.23, 117.59, 116.87, 116.20, 112.06, 108.62, 55.34, 49.06, 42.45, 34.35, 24.59, 21.28, 11.54. **HRMS (ESI):** calcd. for $C_{33}H_{28}BF_2N_8O$ $[M-H]^-$ 601.24257, found 601.24527.

1-(tert-butyl)-3-(4-((3-(5,5-difluoro-7,9-dimethyl-5H-5l4,6l4-dipyrrolo[1,2-c:2',1'-f][1,3,2]diazaborinin-3-yl)propanamido)methyl)phenyl)-5-(4-(piperidin-1-yl)phenyl)-1,2,4-triazin-1-ium 2,2,2-trifluoroacetate (**BODIPY-FL-Trz$^+$**)

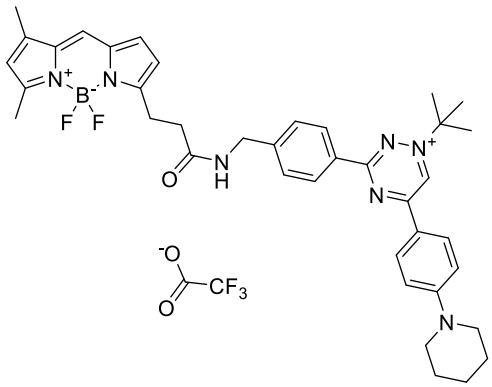

BODIPY-FL (10 mg, 34.24 µmol) and HATU (20 mg, 51.35 µmol) were dissolved in dry DMF (1 mL) and the resulting mixture was left to stir at room temperature for 10 min. Then, triazinium **18** (26 mg, 41.08 µmol) was added followed by addition of DIPEA (42 µL, 239.7 µmol) and the mixture was left to stir for 10 min at room temperature. The reaction was monitored using LCMS. Volatiles were evaporated *in vacuo* and the product was purified using silicagel column chromatography (0-10 % MeOH in DCM with 0.1% TFA). Further purification was needed and therefore RP flash column chromatography (with 0.1 % TFA – HCOOH destroys the product) was used to obtain **BODIPY-FL-Trz$^+$** (10 mg, 37 % yield) as a red solid.**^{1}H NMR (401 MHz, DMSO)**: δ (ppm) = 9.75 (s, 1H), 8.62 (t, *J* = 6.0 Hz, 1H), 8.51-8.42 (m, 4H), 7.71 (s, 1H), 7.54 (d, *J* = 7.9 Hz, 2H), 7.18 (d, *J* = 9.0 Hz, 2H), 7.11 (d, *J* = 3.9 Hz, 1H), 6.39 (d, *J* = 4.0 Hz, 1H), 6.32 (s, 1H), 4.44 (d, *J* = 5.9 Hz, 2H), 3.63 (t, *J* = 5.1 Hz, 4H), 3.15 (t, *J* = 7.8 Hz, 2H), 2.63 (t, *J* = 7.7 Hz, 2H), 2.48 (s, 3H, overlap with DMSO peak), 2.27 (s, 3H), 1.85 (s, 9H), 1.78 – 0.80 (m, 6H). **^{13}C NMR (126 MHz, DMSO)**: δ (ppm) = 171.10, 164.24, 162.67, 159.28, 157.61, 155.00, 145.56, 144.20, 134.50, 132.99, 132.05, 131.18, 128.88, 128.43, 128.02, 125.39, 120.34, 118.35, 116.64, 113.31, 75.13, 47.51, 41.98, 33.79, 28.05, 25.20, 24.03, 23.91, 14.53, 11.02. **HRMS (ESI):** calcd. for $C_{39}H_{45}BF_2N_7O$ $[M]^+$ 676.37412, found 676.37388.

1-(Tert-butyl)-3-(4-((3-(7-(3,4-dimethoxystyryl)-5,5-difluoro-9-methyl-5H-5λ^4,6λ^4-dipyrrolo[1,2-c:2',1'-f][1,3,2]diazaborinin-3-yl)propanamido)methyl)phenyl)-5-(4-(piperidin-1-yl)phenyl)-1,2,4-triazin-1-ium 2,2,2-trifluoroacetate (**19**)

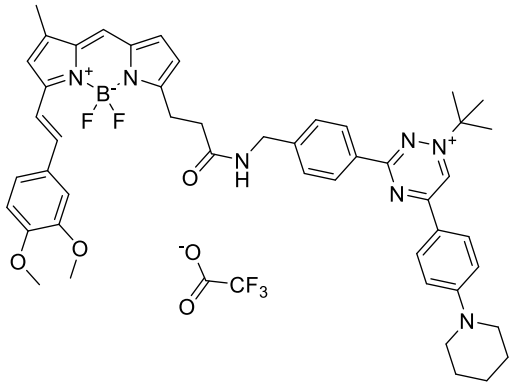

Compound **10** (10 mg, 22.71 µmol) and HATU were dissolved in dry DMF (1 mL) and the resulting mixture was left to stir at room temperature for 10 min. Then, triazinium **18** (17 mg, 27.26 µmol) was added followed by addition of DIPEA (27.7 µL, 159 µmol) and the mixture was left to stir for 5 min at room temperature. The reaction was monitored using LCMS. Volatiles were evaporated *in vacuo* and the product was purified using silicagel column chromatography (0-10 % MeOH in DCM with 0.1% TFA). Further purification was needed and therefore RP flash column chromatography (with 0.1 % TFA – HCOOH destroys the product) was used to obtain compound **19** (15 mg, 55 % yield) as a dark-red solid. **^{1}H NMR (401 MHz, CD$_3$CN)**: δ (ppm) = 9.26 (d, *J* = 2.0 Hz, 1H), 8.55 – 8.39 (m, 2H), 8.33 (dd, *J* = 9.5, 1.9 Hz, 2H), 7.99 – 6.64 (m, 14H), 6.35 (d, *J* = 4.0 Hz, 1H), 4.48 (d, *J* = 6.1 Hz, 2H), 3.90 – 3.79 (m, 6H), 3.61 (s, 3H), 3.24 (t, *J* = 7.6 Hz, 2H), 2.69 (t, *J* = 7.7 Hz, 2H), 2.30 (d, *J* = 9.8 Hz, 4H), 1.85 (s, 9H), 1.74 – 1.62 (m, 6H). **^{13}C NMR (101 MHz, CD$_3$CN)**: δ (ppm) = 172.72, 166.75, 163.52, 158.04, 157.63, 156.53, 152.02, 150.40, 146.74, 144.91, 140.40, 137.40, 135.20, 132.76, 132.33, 129.79, 129.00, 128.46, 123.58, 122.67, 117.44, 116.61, 114.37, 112.73, 110.94, 76.91, 56.44 – 56.33 (m), 48.86, 43.57, 35.21, 28.61, 26.31, 25.12, 11.49. Signals from some of the quaternary carbons were not found, but not enough compound was prepared to repeat the experiments. **HRMS (ESI):** calcd. for $C_{48}H_{53}BF_2N_7O_3$ $[M]^+$ 824.42655, found 824.42655.

(E)-3-(4-((3-(7-(2-(1H-indol-2-yl)vinyl)-5,5-difluoro-9-methyl-5H-5λ^4,6λ^4-dipyrrolo[1,2-c:2',1'-f][1,3,2]diazaborinin-3-yl)propanamido)methyl)phenyl)-1-(tert-butyl)-5-(4-(piperidin-1-yl)phenyl)-1,2,4-triazin-1-ium 2,2,2-trifluoroacetate (**20**)

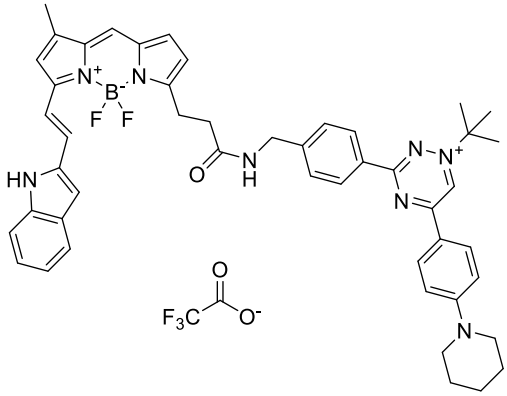

Compound **12** (10 mg, 22.71 µmol) and HATU (13.6 mg, 35.78 µmol) were dissolved in dry DMF (1 mL) and the resulting mixture was left to stir at room temperature for 10 min. Then, triazinium **18** (18.02 mg, 28.62 µmol) was added followed by addition of DIPEA (29 µL, 167.0 µmol) and the mixture was left to stir for 5 min at room temperature. The reaction was monitored using LCMS. Volatiles were evaporated *in vacuo* and the product was purified using silicagel column chromatography (0-10 % MeOH in DCM with 0.1% TFA). Further purification was needed and therefore RP flash column chromatography (with 0.1 % TFA – HCOOH destroys the product) was used to obtain compound **20** (8 mg, 37 % yield) as a bluish dark-red solid. **^{1}H NMR (401 MHz, CD_3CN)**: δ (ppm) = 10.00 (s, 1H), 9.27 (s, 1H), 8.50 – 8.43 (m, 2H), 8.40 – 8.30 (m, 2H), 8.00 (s, 1H), 7.60 – 7.30 (m, 8H), 7.23 – 7.13 (m, 2H), 7.10 – 7.05 (m, 3H), 6.88 (s, 1H), 6.39 (d, *J* = 4.0 Hz, 1H), 4.52 (d, *J* = 6.0 Hz, 2H), 3.63 (t, *J* = 5.2 Hz, 4H), 3.29 (t, *J* = 7.8 Hz, 2H), 2.75 – 2.69 (m, 2H), 2.31 (s, 3H), 1.87 (s, 9H), 1.80 – 1.64 (m, 6H). **^{13}C NMR (101 MHz, CD_3CN)**: δ (ppm) = 172.98, 166.80, 163.57, 156.56, 146.68, 139.68, 136.80, 135.23, 134.68, 132.82, 132.42, 129.86, 129.63, 129.09, 128.58, 125.15, 123.51, 122.03, 121.22, 118.93, 117.87, 117.51, 116.93, 114.45, 112.29, 109.04, 76.96, 48.94, 43.55, 35.21, 28.67, 26.36, 25.38, 25.03, 11.55. **HRMS (ESI):** calcd. for $C_{48}H_{50}BF_2N_8O$ $[M]^+$ 803.41632, found 803.41623.

(4-(6-methyl-1,2,4,5-tetrazin-3-yl)phenyl)methanol (**22**)

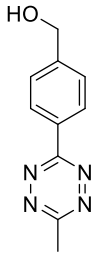

4-(hydroxymethyl)benzonitrile **21** (500 mg, 3.76 mmol) and $Zn(OTf)_2$ (683 mg, 1.88 mmol) were dissolved in dry MeCN (1.96 mL, 37.55 mmol). Then, hydrazine monohydrate (9.11 mL, 187.8 mmol) was added and the reaction mixture was left to stir for 65 h at 60 °C under argon atmosphere. Then, sodium nitrite (5.18 g, 75.1 mmol) was added to the reaction, followed by addition of 2M HCl aqueous solution until pH ~ 3. (This step generates **highly toxic** nitrogen oxide gases and should be performed in a well ventilated fume hood).[52] The reaction mixture was extracted with DCM (4x50 mL) and the combined organic fractions were dried over $MgSO_4$. The volatiles were removed *in vacuo* and the

product was purified using silicagel column chromatography (PE/AcOEt 1/1) to give compound **22** (240 mg, 32 % yield) as a pink solid. **^{1}H NMR (401 MHz, $CDCl_3$)**: δ (ppm) = 8.87 – 8.44 (m, 2H), 7.71 – 7.48 (m, 2H), 4.84 (d, *J* = 5.8 Hz, 2H), 3.10 (s, 3H), 1.86 (t, *J* = 5.9 Hz, 1H). Spectra are in accordance with literature.[52]

4-(6-methyl-1,2,4,5-tetrazin-3-yl)benzaldehyde (**23**)

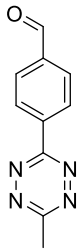

Compound **22** (232 mg, 1.15 mmol) and Dess-Martin periodinane (535 mg, 1.26 mmol) were dissolved in dry DCM (10 mL) and the reaction was left to stir for 1.5 h at r.t. under argon atmosphere. Then, volatiles were evaporated and the crude product was purified by silica column chromatography (PE/EA 2/1 - 1/1) to give compound **23** as a dark red solid (221 mg, 96 % yield). **^{1}H NMR (401 MHz, $CDCl_3$)**: δ (ppm) = 10.16 (s, 1H), 8.86 – 8.71 (m, 2H), 8.22 – 7.93 (m, 2H), 3.15 (s, 3H). Spectra are in accordance with literature.[54]

(E)-3-(5,5-difluoro-9-methyl-7-(4-(6-methyl-1,2,4,5-tetrazin-3-yl)styryl)-5H-5λ^4,6λ^4-dipyrrolo[1,2-c:2',1'-f][1,3,2]diazaborinin-3-yl)propanoic acid (**24**)

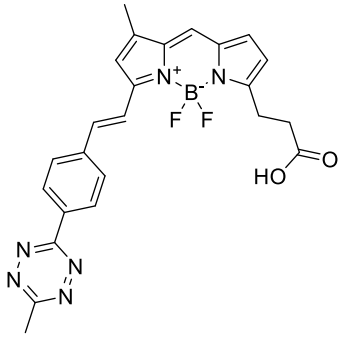

BODIPY-FL (20 mg, 69,5 µmol) and compound **23** (82 mg, 411 µmol) were dissolved in dry MeCN (5 mL) under argon atmosphere. Then, acetic acid (39 µL, 685 µmol) and pyrrolidine (57 µL, 685 µmol) were added and the reaction was left to stir for 2.5 h at r.t. under argon atmosphere. Subsequently, the solvent was removed by a flow of nitrogen followed by placing the reaction vessel under high vacuum to remove all volatiles including pyrrolidine and acetic acid. Then, the crude product was dissolved in 1 mL of MeCN and loaded onto a RP column (20-100 % MeCN in water with 0.05 % formic acid) to give compound **24** (4.0 mg, 12 % yield) as a purple solid. **^{1}H NMR (401 MHz, DMSO)**: δ (ppm) = 8.60 – 8.50 (m, 2H), 7.95 – 7.84 (m, 2H), 7.82 – 7.71 (m, 2H), 7.59 (d, *J* = 16.5 Hz, 1H), 7.18 (d, *J* = 4.1 Hz, 1H), 7.13 (d, *J* = 1.2 Hz, 1H), 6.48 (d, *J* = 4.0 Hz, 1H), 3.15 (dd, *J* = 8.9, 6.7 Hz, 2H), 3.06 – 2.98 (m, 3H), 2.75 – 2.63 (m, 2H), 2.34 (s, 3H). **^{13}C NMR (101 MHz, DMSO)**: δ (ppm) = 173.91, 167.46, 163.42, 158.89, 154.93, 143.57, 140.02, 137.43, 136.40, 134.54, 132.80, 130.75, 130.06, 128.65 (d, *J* = 3.3 Hz), 125.07, 120.15, 118.00, 117.56, 32.67, 24.25, 21.34, 11.58. **HRMS (ESI):** calcd. for $C_{24}H_{20}BF_2N_6O_2$ $[M-H]^-$ 473.17143, found 473.17132.

8.3 Live-cell experiments – methodologies

*8.3.1 **BCN-TPP** mitochondrial labeling*

U2OS (H2B SPARK) cells were seeded on a 96-well plate at a density of 17500 cells per well in a complete DMEM medium. After 48h incubation, the cells were incubated with 5 µM ***endo*-BCN-TPP** complete DMEM medium for 15 min.[48] The cells were washed 3 times with a complete L-15 medium. After that, 1 µM of each cell-permeable fluorogenic probe was added to the cells in a complete L-15 medium (non-red-shifted probe **BODIPY-FL-Trz$^+$** also with addition of DRAQ5 (5 µg/mL)) for 30 min . Then the cells were imaged on a confocal microscope without any washing (Figure 18, Figure 20).

8.3.2 Model drug's cellular labeling

U2OS (H2B SPARK) cells were seeded on a 96-well plate at a density of 17 500 cells per well in a complete DMEM medium. After 48h incubation, the cells were incubated with 2 µM Dasatinib-PEG3-BCN (Dasatinib-BCN) in complete DMEM for 2 h.[48] The cells were washed 3 times with a complete L-15 medium. After that, 1 µM of each cell-permeable fluorogenic probe was added to the cells in a complete L-15 medium (non-red-shifted probe **BODIPY-FL-Trz$^+$** also with addition of DRAQ5 (5 µg/mL)) for 30 min. Then the cells were imaged on a confocal microscope without washing (Figure 19, Figure 21).

Acknowledgements

I would like to express my sincere gratitude to my group leader, Dr. Milan Vrábel, for his guidance and support throughout my years in his group. His expertise and encouragement were essential in shaping this work.

I am especially grateful to my colleague and consultant, Dr. Paul Reyes, for his generous help in times of need both in practical aspects of my research and in writing this thesis. I am also thankful to my colleague Ing. Marek Chovanec for his help in the making of this work. Special thanks go to Dr. Veronika Šlachtová for taking her time and conducting the biological experiments with my compounds. I also thank our whole research team for creating a pleasant work environment.

Lastly, I want to express my sincere gratitude to my family and my girlfriend for their unconditional love and support throughout the years.

5. Literature

(1) Nadler, A.; Schultz, C. *Angew. Chem. Int. Ed*. **2013**, *52* (9), 2408–2410.

(2) Hang, H. C.; Yu, C.; Kato, D. L.; Bertozzi, C. R. *Proc Natl Acad Sci U S A*. **2003**, *100* (25), 14846–14851.

(3) Chen, L.; Li, F.; Li, Y.; Yang, J.; Li, Y.; He, B. *Chem commun*. **2021**, *58* (2), 298–301.

(4) Wang, L.; Frei, M. S.; Salim, A.; Johnsson, K. *J Am Chem Soc*. **2019**, *141* (7), 2770–2781.

(5) Dedecker, P.; De Schryver, F. C.; Hofkens, J. *J. Am. Chem. Soc*. **2013**, *135*.

(6) Minta, A.; Kao, J. P. Y.; Tsien, R. Y. *J Biol Chem*. **1989**, *264* (14), 8171–8178.

(7) Hang, H. C.; Yu, C.; Kato, D. L.; Bertozzi, C. R. *Proc Natl Acad Sci U S A*. **2003**, *100* (25), 14846–14851.

(8) Carell, T.; Vrabel, M. *Top Curr Chem*. **2016**, *374* (1).

(9) Kozma, E.; Kele, P. *Top Curr Chem.* **2024**, *382* (1), 1–31.

(10) Bird, R. E.; Lemmel, S. A.; Yu, X.; Zhou, Q. A. *Bioconjug Chem*. **2021**, *32* (12), 2457–2479.

(11) Blackman, M. L.; Royzen, M.; Fox, J. M. *J Am Chem Soc*. **2008**, *130* (41), 13518–13519.

(12) Devaraj, N. K.; Hilderbrand, S.; Upadhyay, R.; Mazitschek, R.; Weissleder, R. *Angew. Chem. Int. Ed*. **2010**, *49* (16), 2869–2872.

(13) Carlson, J. C. T.; Meimetis, L. G.; Hilderbrand, S. A.; Weissleder, R. *Angew. Chem. Int. Ed*. **2013**, *52* (27), 6917–6920.

(14) Fang, Y.; Hillman, A. S.; Fox, J. M. *Top Curr Chem.* **2024**, *382* (2), 1–63.

(15) Shen, T.; Liu, X. *Chem Sci*. **2025**, *16* (11), 4595–4613.

(16) Werther, P.; Yserentant, K.; Braun, F.; Grußmayer, K.; Navikas, V.; Yu, M.; Zhang, Z.; Ziegler, M. J.; Mayer, C.; Gralak, A. J.; Busch, M.; Chi, W.; Rominger, F.; Radenovic, A.; Liu, X.; Lemke, E. A.; Buckup, T.; Herten, D. P.; Wombacher, R. *ACS Cent Sci*. **2021**, *7* (9), 1561–1571.

(17) Choi, S.-K.; Kim, J.; Kim, E.; Choi, S.-K. ; Kim, J. ; Kim, E.; Hierso, J.-C. *Molecules*. **2021**, *26*, 1868.

(18) Forster, T. *Naturwissenschaften*. **1946**, *33* (6), 166–175.

(19) Dexter, D. L. *J Chem Phys*. **1953**, *21* (5), 836–850.

(20) Speiser, S. Chem. Rev. **1996**, 96 (6), 1953–1976.

(21) Fan, J.; Hu, M.; Zhan, P.; Peng, X. *Chem Soc Rev*. **2012**, *42* (1), 29–43.

(22) Chi, W.; Huang, L.; Wang, C.; Tan, D.; Xu, Z.; Liu, X. *Mater Chem Front*. **2021**, *5* (18), 7012–7021.

(23) Shen, T.; Zhang, W.; Yadav, P.; Sun, X. W.; Liu, X. *Mater Chem Front*. **2023**, *7*, 1082.

(24) Shen, T.; Liu, X. *Chem Sci*. **2025**, *16* (11), 4595–4613.

(25) Pinto-Pacheco, B.; Carbery, W. P.; Khan, S.; Turner, D. B.; Buccella, D. *Angew. Chem. Int. Ed*. **2020**, *59* (49), 22140–22149.

(26) Mao, W.; Chi, W.; He, X.; Wang, C.; Wang, X.; Yang, H.; Liu, X.; Wu, H. *Angew. Chem. Int. Ed*. **2022**, *61* (22), e202117386.

(27) Dommerholt, J.; Schmidt, S.; Temming, R.; Hendriks, L. J. A.; Rutjes, F. P. J. T.; Van Hest, J. C. M.; Lefeber, D. J.; Friedl, P.; Van Delft, F. L. *Angew. Chem. Int. Ed*. **2010**, *49* (49), 9422–9425.

(28) Peterson, J. A.; Wijesooriya, C.; Gehrmann, E. J.; Mahoney, K. M.; Goswami, P. P.; Albright, T. R.; Syed, A.; Dutton, A. S.; Smith, E. A.; Winter, A. H. *J Am Chem Soc*. **2018**, *140* (23), 7343–7346.

(29) Poryvai, A.; Galkin, M.; Shvadchak, V.; Slanina, T. *Angew. Chem. Int. Ed*. **2022**, *61* (34), e202205855.

(30) Rao, D. N.; Ji, X.; Miller, S. C. *Chem Sci*. **2022**, *13* (20), 6081–6088.

(31) *Rhodamine B for fluorescence 81-88-9*. https://www.sigmaaldrich.com/CZ/en/product/sigma/83689?srsltid=AfmBOoovHf6sE4GnSIuxTt2nhADXPucuItXA1P_IzGlCZZZyJ73WPd2f (accessed 2025-05-02).

(32) Ohno, H.; Sasaki, E.; Yamada, S.; Hanaoka, K. *Org Biomol Chem*. **2024**, *22* (16), 3099–3108.

(33) Ulrich, G.; Ziessel, R.; Harriman, A. *Angew. Chem. Int. Ed*. **2008**, *47* (7), 1184–1201.

(34) *BODIPY FL-NHS ester ≥98% (HPLC) | Sigma-Aldrich*. https://www.sigmaaldrich.com/CZ/en/product/sigma/sml3990 (accessed 2025-03-20).

(35) *Cyanine 3 Phosphoramidite - 2-[3-[1,3-Dihydro-1-[3-(4-methoxytriphenylmethoxy)propyl]-3*.

https://www.sigmaaldrich.com/CZ/en/substance/cyanine3phosphoramidite9181771859 4662 (accessed 2025-03-20).

(36) Katoh, T.; Yoshikawa, M.; Yamamoto, T.; Arai, R.; Nii, N.; Tomata, Y.; Suzuki, S.; Koyama, R.; Negoro, N.; Yogo, T. *Bioorg Med Chem Lett*. **2017**, *27* (5), 1145–1148.

(37) Li, Y.; Fu, H. *ChemistryOpen*. **2020**, *9* (8), 835–853.

(38) Kamber, D. N.; Liang, Y.; Blizzard, R. J.; Liu, F.; Mehl, R. A.; Houk, K. N.; Prescher, J. A. *J Am Chem Soc*. **2015**, *137* (26), 8388–8391.

(39) Park, J.; Hahm, J.; Yim, J.; Lee, H.; Hwang, H. M.; Lee, S.; Park, J.-Y.; Velladurai, A.; Gangasani, J. K.; Cho, H.; Park, H.; Lee, M.; Lee, J.; Eom, H.; Song, W. J.; Lee, S.; Kim, E.; Park, J. *ACS Cent Sci*. **2025**.

(40) Šlachtová, V.; Bellová, S.; La-Venia, A.; Galeta, J.; Dračínský, M.; Chalupský, K.; Dvořáková, A.; Mertlíková-Kaiserová, H.; Rukovanský, P.; Dzijak, R.; Vrabel, M. *Angew. Chem. Int. Ed*. **2023**, *62* (36).

(41) Šlachtová, V. ; Bellová, S.; Vrabel, M. *Cite This: J. Org. Chem*. **2024**, *89*.

(42) Šlachtová, V.; Bím, D.; Németh, K.; Barańska, E.; Bellová, S.; Dračínský, M.; Dzijak, R.; Kele, P.; Slanina, T.; Vrabel, M. **2025**. (Article in preparation).

(43) Katoh, T.; Yoshikawa, M.; Yamamoto, T.; Arai, R.; Nii, N.; Tomata, Y.; Suzuki, S.; Koyama, R.; Negoro, N.; Yogo, T. *Bioorg Med Chem Lett*. **2017**, *27* (5), 1145–1148.

(44) Black, P. J.; Cami-Kobeci, G.; Edwards, M. G.; Slatford, P. A.; Whittlesey, M. K.; Williams, J. M. J. *Org Biomol Chem*. **2006**, *4* (1), 116–125.

(45) Agramunt, J.; Ginesi, R.; Pedroso, E.; Grandas, A. *J. Org. Chem*. **2020**, *85* (10), 6593–6604.

(46) Scott, J. I.; Mendive-Tapia, L.; Gordon, D.; Barth, N. D.; Thompson, E. J.; Cheng, Z.; Taggart, D.; Kitamura, T.; Bravo-Blas, A.; Roberts, E. W.; Juarez-Jimenez, J.; Michel, J.; Piet, B.; de Vries, I. J.; Verdoes, M.; Dawson, J.; Carragher, N. O.; Connor, R. A. O.; Akram, A. R.; Frame, M.; Serrels, A.; Vendrell, M. *Nat Commun*. **2022**, *13* (1), 2366.

(47) Wang, Y.; Yang, H.; Li, J.; Kong, Q.; Zhou, S.; Sun, H.; Pan, L.; Gong, Q.; Feng, P.; Wu, H. *Chinese Chem Lett*. **2024**, *35* (8), 109226.

(48) Siegl, S. J.; Galeta, J.; Dzijak, R.; Dračínský, M.; Vrabel, M. *Chempluschem*. **2019**, *84* (5), 493–497.

(49) Smith, R. A. J.; Porteous, C. M.; Gane, A. M.; Murphy, M. P. *Proc Natl Acad Sci U S A*. **2003**, *100* (9), 5407–5412.

(50) Olivieri, A.; Manzione, L. *Ann Oncol*. **2007**, *18* (SUPPL. 6), vi42–vi46.

(51) Black, Phillip. J.; Cami-Kobeci, G.; Edwards, M. G.; Slatford, P. A.; Whittlesey, M. K.; Williams, J. M. J. *Org. Biomol. Chem.* **2006**, *4* (1), 116–125.

(52) Yang, J.; Karver, M. R.; Li, W.; Sahu, S.; Devaraj, N. K. *Angew. Chem. Int. Ed*. **2012**, *51* (21), 5222–5225.

(53) Bertheussen, K.; van de Plassche, M.; Bakkum, T.; Gagestein, B.; Ttofi, I.; Sarris, A. J. C.; Overkleeft, H. S.; van der Stelt, M.; van Kasteren, S. I. *Angew. Chem. Int. Ed*. **2022**, *61* (38), e202207640.

(54) Werther, P.; Möhler, J. S.; Wombacher, R. *Chem - Eur J*. **2017**, *23* (72), 18216–18224.